Interactive comment on "**The fate of upwelled nitrate off Peru shaped by submesoscale filaments and fronts**" *by* **Jaard Hauschildt et al.**

Takeyoshi Nagai (Referee)

takeyoshi@gmail.com
Received and published: 1 June 2020

This study investigates the effects of filaments and fronts on subduction of nitrate in the Peru-Chile Upwelling System, using a submesoscale permitting regional ocean model coupled with a biogeochemical model. The results of this study found that about 40% of the newly upwelled nitrate near the coast of Peru is subducted before being used by phytoplankton. The results show a more pronounced subduction occurs at submesoscale fronts near the cold filaments, which were underestimated by the previous mesoscale resolving models. The manuscript is well written and includes new insights on the subduction of the nitrate in EBUS. Therefore, I have only several minor comments below.

Reply: The authors would like to thank Takeyoshi Nagai for his overall favorable review of our manuscript and his detailed, constructive comments which helped to improve the paper.

P1L11 "highlighting the additional value of direct rate measurements for model validation. " Unclear

Reply: This sentence has been rephrased and now reads as follows:

P1L9-11: "Surface chlorophyll in the filament is a factor 4 lower than at the upwelling front while surface primary production is a factor 2 higher."

P2L13 "citepChavez2007, Gruber2015, Koehn2017, Brady2019. " Typo

P11L8 "80m (100m)" Spaces are needed before "m".

P11L29 "30km" A space is needed before "km".

Reply: These mistakes have been corrected in the new manuscript.

P11L30 "...along-shore position matches with two SST minima (16 âŮe̡ C) at the coast..." I couldn't find two SST minima 16 degree at the coast in Figure 2. From the color scale they look like 18-19 degree.

Reply: We mistakenly described the SST minima of the model simulation instead of the observations in this sentence, the temperature has been changed to reflect the observed values. It now reads as follows:

P16L33-34: "Their along-shore position matches with two SST minima (19°C) at the coast, suggesting that they carry recently upwelled water."

P14L2 ". . .is characterized in the following. . ." "is" should be "are".

Reply: This mistake has been corrected in the new manuscript. It now reads as follows:

P18L4-5: "The physical structure of the filament and the distribution of the biogeochemical parameters are characterized in the following."

Figure 3 and 4 captions There is no explanation for the broken white lines, which are probably MLD by reading legend, but the information should be in the captions.

Reply: The broken white lines indeed represent the mixed-layer depth as stated in the legend, the information has been added to the captions as well (Note that these figures are now Figures 4 and 5 due to the addition of Figure 2 for validation purposes following another reviewer's comment).

P17L28 "In brief, in situ PP observations based on carbon suggest that a significant portion of the observed offshore reduction in nitrate concentrations is due to uptake by PP. Simulations indicate that approximately 40.6% of upwelled nitrate is subducted and not utilised by PP. " Is this because PP estimated in-situ without the effect of subduction of nitrate?

Reply: Thank you for this interesting comment. The in-situ PP estimate is computed using water samples contained in a bottle (as detailed in section 2.3). At the time and depth the bottle is closed, there is no way to determine whether the sampled water mass is a subducted water mass. To determine PP for a subducted water mass, it would be necessary to follow the water mass before it is sampled and be able to know that it has subducted. This was not done in the Eulerian experimental setup here and would require a Lagrangian approach. We can only assume that the sampled water mass corresponds to the filament and thus likely corresponds to a subducted water mass.

P19L32 "While the coincidence of increased subduction and a negative change in nitrate may seem counterintuitive, ..." To me, increased subduction and reduction of nitrate are not counterintuitive.

Reply: We agree that to readers who are very familiar with the key concepts of our paper the use of the word "counterintuitive" seems out of place and is not needed. We rephrased the sentence as follows:

P24L8-10: "The positive change in nitrate offshore together with increased eddy kinetic energy (EKE) in the 1/45° simulation suggests that an increase in the cross-shore nitrate flux takes over once the nitrate is removed from the surface (Fig. 8a,b)."

P20L2 "−2 " Is the minus sign here for an increase?

Reply: The minus sign was a typo and has been fixed, the corrected sentence is:

P24L11-12: "At a depth of 300 m to 500 m nitrate increases near the coast (~ 2 µmol l⁻¹), directly below the strong negative nitrate change in the top 200 m (~ −2.75 µmol l⁻¹)."

P20L3 "A plausible explanation for this pattern is that organic matter is able to sediment at shallower depth on the slope in the mesoscale simulation, which permits enhanced local remineralization and nitrate release with respect to the submesoscale simulation. " I'm confused. If this is the case, remineralized nitrate is higher in 1/9 degree simulation with negative value in Figure 7b in below 300 m near the coast?

Reply: We agree that the formulation in the first manuscript version was confusing. We now describe changes in the submesoscale simulation relative to the mesoscale simulation. The key concept that was missing from our previous process description is that due to increased offshore transport in the submesoscale simulation sinking organic matter sediments at deeper shelf areas, out of reach of the upwelling source waters. This results in a downward redistribution of nitrate similar to the „nutrient leakage" described in Gruber et al. 2010, a reference that we also added at this point in the manuscript. We rephrased our explanation:

P24L12-P25L4: "A plausible explanation for this pattern is that due to increased offshore transport in the submesoscale simulation sinking organic matter sediments on deeper shelf areas, out of reach of the upwelling source waters. This would result in a downward redistribution of nitrate similar to the "nutrient leakage" described in Gruber et al. (2011). However, small differences in the alongshore mean circulation along the continental slope (not shown) may also modify the nitrate content of the water masses. Disentangling these processes is beyond the scope of the present work."

P23L7 "Along-shore variability of PP in the simulations is closely related to chlorophyll concentrations, while the observed relationship of PP and chlorophyll is clearly more complex (Table 1). Investigating the reasons for this discrepancy is

beyond the scope of this study and left for future work " Is this because PP estimated in-situ without the effect of subduction to dark layers?

Reply: As explained in the reply to a previous comment, our experimental setup is not able to determine accurately whether the sampled water mass is a subducted water mass or not. So there is a possibility that the measured PP corresponds to the PP in an upwelled water mass or a subducted one. Another plausible explanation for these differences might be that despite the already high complexity in a model like PISCES, the parameterisation of primary production is still relatively simple. For example, changes of the phytoplankton physiology or species composition of the phytoplankton community are not modelled. Another missing process is the aging or health of the phytoplankton population, since in the real ocean phytoplankton does not change its state from „alive and containing chlorophyll" to „dead organic matter without chlorophyll" instantly. Some intermediate stage where the phytoplankton population may be hardly growing on average but still contains some chlorophyll seems more realistic, but it is not represented in this version of the PISCES model (note that a new version, PISCES-quota (Kwiatkowski et al., 2018) will be able to represent more elaborated phytoplankton stages in future studies). We have also incorporated this point into the discussion:

P28L30-P29L3: "Along-shore variability of PP in the simulation is closely related to chlorophyll concentrations, while the observed relationship of PP and chlorophyll is less clear (Table 1). Investigating the reasons for this discrepancy is beyond the scope of this study and left for future work, but we can speculate that it is related to the relatively simple parameterisation of primary production in PISCES (see section 2.5). For example, changes of the phytoplankton physiology or species composition of the phytoplankton community are not modelled. Another missing process is the aging or health of the phytoplankton population, which could slow down PP while chlorophyll concentrations remain high and thereby decouple both parameters. Note that a new version, PISCES-quota (Kwiatkowski et al., 2018) will be able to represent more elaborate phytoplankton stages in future studies."

Ref: Kwiatkowski, L., Aumont, O., Bopp, L., & Ciais, P. (2018). The Impact of variable Phytoplankton Stoichiometry on Projections of primary production, food quality, and carbon uptake in the global ocean. *Global Biogeochemical Cycles*, *32*(4), 516-528.

P23L13 "Near-surface stratification in the model is by a factor of 2-3 lower than in the observations " What mixing parameterization used in this study is missing in the manuscript. Is it KPP or two-equation type turbulence closures?

Reply: The KPP parameterization is used. We added this information in the model description section:

P6L29-30: "The nonlocal K-Profile Parameterization (KPP) scheme is used to handle unresolved processes related to vertical mixing."

P23L18-31 "However, the fact that nitrate concentration..." I think that PISCES includes ammonium. Therefore, the authors can see the fraction of ammonium for the PP.

Reply: The PISCES model indeed includes ammonium. However, the sentence in question refers to our rate measurements which do not distinguish between new production and regenerated production. Since we have no observations to evaluate / compare the regenerated production in the model, we decided to only report total primary productivity. We rephrased the sentence slightly to make it very clear that this statement refers to observations only.

P28L13-18: "Besides, our observations of PP rates in the filament do not distinguish between regenerated production from ammonium and new production from nitrate (Dugdale and Goering, 1967). Fernández et al. (2009) show that regenerated nitrogen can locally account for as much as 50% of surface primary production in southern Peru. However, nitrate concentrations measured in the filament 150 km offshore are only 20 - 50% of those measured near the coast and nitrate appears to decrease with offshore distance on transect CROSS (Fig. 4). This is an indicator that a substantial amount of PP in the region of the filament survey near 15°S is fuelled by newly upwelled nitrate."

Interactive comment on **"The fate of upwelled nitrate off Peru shaped by submesoscale filaments and fronts"** *by* **Jaard Hauschildt et al.**

Anonymous Referee #2

Received and published: 24 July 2020

The authors present a study that combines observations and modeling in order to assess the role of submesoscale filaments and fronts in the lateral and vertical redistribution of the upwelled nutrients. They use ship data collected both along shore and cross shore transects off the coast of Peru to study the structure of upwelling filaments and their role in the nutrient transport and subduction, and its impact on primary production. Further, they use a coupled CROCO+PISCES simulation to strengthen these findings and expand their analysis through lagrangian experiments that allow them to follow the biogeochemical transformations of upwelled particles. They find that sub- mesoscale filaments adevect upwelled nutrients offshore, while also subducting them, therefore limiting production.

The paper is interesting and contains relevant in situ data on these submesoscale structures. I appreciated the Lagrangian approach to study biogeochemical transformations and the fate of the upwelled particles. The results are interesting: they strengthen previous claims regarding the importance of filaments and fronts for the offshore transport, while clarifying better the role of these structures in the enhancement of subduction (rather than submesoscale upwelling). The writing is good, with a few typos and some potential for improving the paper structure (see comments below).

I have two major comments that I'm listing below, plus a few minor/detailed comments following. My main concerns regard: lack of a thorough model evaluation, lack of a clear description of the biogeochemical model and therefore of the meaning of certain processes the authors refer to to draw conclusions. I also have a few concerns regarding the paper structure, which I am listing in the detailed comments as they refer to some specific sections. I suggest that the paper is published after revisions are done.

Reply: The authors would like to thank Referee #2 for the very thorough and fair review of our manuscript. We have taken into account the reviewer's comments and we believe this resulted in substantial improvements of our original manuscript. In particular we followed both major suggestions of the reviewer: we added a thorough model evaluation (i.e. a new figure with a Taylor diagram) and a clear description of the nitrate uptake within the biogeochemical model. All changes are outlined in detail below.

MAJOR COMMENTS

1) Model evaluation

In my opinion, the paper lacks a thorough model evaluation. Was this exact model setup and run used in a previous publication, where a full evaluation can be found? Is there an appendix or supplementary material that I missed containing more information in this regard? If this is not the case, I strongly encourage the authors to provide a better evaluation of the model, as the current information doesn't seem enough to me. The only figures that provide some comparison between model and observations are Figure 2, 3, 4. However, these images refer to specific days (April 14 2017 and April 5 2017 respectively in observations and model), and they seem to show pretty large biases in the temperature and salinity fields in the model, especially in the upwelling area. These are accompanied by very high nutrient levels, suggesting a high bias in the upwelling fluxes overall. Both the physical and biochemical tracer biases can have important repercussions on the lateral and vertical fluxes and transformations which require to be discussed in the paper discussion section as they may impact the results of the Lagrangian analysis. No longer term mean evaluation of the model is explicitly provided (even though the model was run for several years). Also, the discussion of the model performance in the paper text is too qualitative and scattered throughout the text, while it would be worth having a dedicated subsection. I strongly suggest that the authors include in the paper some difference plots (SST, SSS, MLD, velocities, EKE, CHL, nutrients) and/or use a Taylor diagram to summarize the performance of the model in the region of study in order to be able to assess its limitations in the discussion.

Reply: We agree that the omission of a thorough model evaluation was an oversight on our part. Note that a thorough validation of the model has been carried out in the first author's Master's Thesis (Hauschildt 2017) which was based on the same simulations. However we agree with the review that the validation should also be included in this peer-reviewed publication. The mesoscale 1/9° model is essentially the same configuration that is used in Echevin et al. 2013, but we agree that at the very least this would need to be clarified in the text.

Based on your remarks we now include one figure quantifying the model fit of the most relevant parameters (CHL, SST, NO3) with Taylor diagrams in the main manuscript. This is done for both the mesoscale and submesoscale model configurations. We don't want to lengthen the main paper too much and reduce the readability with the model evaluation, thus we included further information as supplementary material (Figure S1 with average horizontal maps used to compute statistics for Figure 2a,b). We now also refer to the Master Thesis for readers who are interested in even more details.

Ref.: Hauschildt, J. (2017) *Observed and modeled biogeochemistry of filaments off Peru.* **(Master thesis), Christian-Albrechts-Universität Kiel, Kiel, Germany, 110 pp. DOI [10.13140/RG.2.2.18259.48162](http://oceanrep.geomar.de/41369). http://oceanrep.geomar.de/41369"**

We also discuss in detail in several new paragraphs the impact of the subsurface nitrate bias on the amount of nitrate that is subducted (P25L21 - P27L29). We conclude that our approach tends to slightly overestimate the fraction of subducted nitrate.

2) Biogeochemical model

Throughout the text, the authors refer to key biogeochemical processes resolved by the model PISCES. However, these processes are never well defined in terms of what other modeled processes and variables they depend upon, and which quantities drive and regulate them in the model. Sometimes assumptions are made regarding modeled biogeochemical processes, when the way they work should be known from the model equations. Please, include an explicit description of the few relevant model processes in your methods section, and clarify to the reader how they relate to each other, providing fundamental knowledge regarding the characteristics of the employed bio-geochemical model. Example 1: in page 15, lines 10-16, the authors discuss the fact that chlorophyll and production relate differently to each other in model and observations; this depends on the model code, which is known, and therefore the question is: how does PP relate to CHLA in the model? Can you explain these differences using the model equations, since they can be checked, and is it worth suggesting any amendment to the processes represented by the model given what you find in the observations? Since this process is of interest, the authors should include more information on the model representation of these processes in the methods. Example 2: page 15, lines 29-30: The authors talk about modeled primary production and nitrate uptake, however no information was provided to understand how the two relate to each other in the model. What processes contribute to nitrate uptake in PISCES?

Reply: Given that the differences in CHL and PP between simulation and observations are a major part of our discussion, we totally agree that a description of how PP and nitrate uptake are parameterised in PISCES should be part of the manuscript. We added a corresponding paragraph to the methods (section 2.5, P8L14-P9L13) which is then referenced in the discussion.

DETAILED COMMENTS
Page 2, line 10-11: This sentence is too long, please split it in two parts.

Reply: We split this sentence as follows and added also two more references related to organic matter remineralization and oxygen consumption off Peru:

P2L9-12: "Furthermore, the high productivity and export of organic matter and its subsequent remineralization at depth result in high oxygen consumption (Kalvelage et al. 2015, Loginova et al. 2018). In combination with poor ventilation by sluggish currents this leads to the presence of the shallowest and most intense oxygen minimum zone (OMZ) in the global ocean (Wyrtki, 1962; Paulmier et al., 2006; Karstensen et al., 2008; Stramma et al., 2010)."

Page 2, line 34: Please add the following modeling study for the filament transport in the Canary Upwelling System: Lovecchio, E., Gruber, N., & Münnich, M. (2018). Mesoscale contribution to the long-range offshore transport of organic carbon from the Canary Upwelling System to the open North Atlantic. Biogeosciences, 15(16), 5061- 5091.

Reply: This relevant suggested reference was added.

P2L32: "Previous studies have attempted to quantify the fluxes of biogeochemical tracers related to eddies and filaments in EBUS using biogeochemical models of various complexity (e.g. Nagai et al., 2015 in the California EBUS; Frenger et al., 2018; Montes et al., 2014; Bettencourt et al., 2015; José et al., 2017 in the PCUS; Lovecchio et al., 2018 in the Canary EBUS)."

Page 3, line 6-7: Please rephrase the following sentence "For instance, if nitrate uptake by PP occurred much faster than subduction, then mainly organic matter produced in the surface layer would be subducted, whereas if it were slower, nitrate would be subducted. "

Reply: We rephrase this sentence as follows:

P3L6-8: "For instance, if the time scale of nitrate uptake by PP was shorter than that of subduction, mainly organic matter produced in the surface layer would be subducted. If it were longer, mainly nitrate would be subducted."

Page 3, line 9: What does "process studies" mean?

Reply: What is typically meant by this is the following: A process study aims to increase the understanding of a particular process. In our case it is the subduction of nitrate by submesoscale turbulence. Typically process studies are carried out over shorter time periods compared to long term observations or monitoring activities which mainly aim to document the mean state and its variability. Regardless, we removed the term process study to avoid confusion:

P3L10-12: "Dedicated studies combining multi-disciplinary observations with modelling efforts at meso- and submesoscale are key to advance our

understanding of complex physical-biogeochemical interactions (Oschlies et al., 2018).”

Page 3, line 23: Is 2.5 km resolution enough to resolve submesoscale? I thought one needed at least 2 km, if not 1 km. Could you please refer to literature to confirm your statement that 2.5 km is enough?

Reply: Absolute kilometer scales are not adequate to describe how much of the submesoscale spectrum is resolved. The comparison of the effective model resolution with the local Rossby Radius is more useful. Since the Peruvian upwelling system is located relatively close to the equator and the Coriolis parameter is therefore small, the Rossby radius (effectively the limit of quasi-geostrophic / mesoscale dynamics) is ~60 km (Chelton et al., 1998), an order of magnitude larger than our 2.5 km model resolution. However, we cannot claim that this model resolves all submesoscale processes. Much higher resolution on the order of 100 m would be needed to resolve e.g. symmetric instability (Thomas et al., 2008). This is precisely the reason why we call our simulation submesoscale-permitting instead of submesoscale-resolving. Only features at the upper end of the submesoscale variability spectrum such as frontal structures and filaments are resolved at this resolution, but these are the key features for subduction. We are therefore confident that our results are of interest with respect to the dynamical features and processes that we are describing. We have added a sentence relating our horizontal model resolution to the Rossby radius to the methods, section 2.5:

P7L4-7: “Since the Peruvian upwelling system is located relatively close to the equator, the Rossby radius is ~ 60 km (Chelton et al., 1998), an order of magnitude larger than our model resolution (~ 2.5 km). The Rossby radius represents effectively the limit of mesoscale dynamics and we can thus consider our model submesoscale-permitting, as it resolves the upper range of the submesoscale variability spectrum.”

Chelton, D.B., DeSzoeke, R.A., Schlax, M.G., El Naggar, K. and Siwertz, N., 1998. Geographical variability of the first baroclinic Rossby radius of deformation. *Journal of Physical Oceanography*, *28*(3), pp.433-460, https://doi.org/10.1175/1520-0485(1998)028<0433:GVOTFB>2.0.CO;2

Thomas, L. N., Tandon, A., and Mahadevan, A.: Submesoscale Processes and Dynamics, in: Ocean Modeling in an Eddying Regime, edited by Hecht, M. W. and Hasumi, H., pp. 17–38, American Geophysical Union, https://doi.org/10.1029/177GM04, 2008

Page 3, line 26, point nr.1: As I stated, I don’t think the paper answers this question, because the model evaluation in the paper is extremely limited and restricted to a few

specific simulated events rather than the mean state of the system and its dynamics. Also this is more of a model evaluation problem than a scientific question. I wouldn't include question nr 1 here, I would only leave questions nr 2 and 3.

We agree and have omitted this question from the introduction.

Subsection 2.5: Please provide here a description of how the relevant processes discussed in the paper are represented by the biogeochemical model PISCES. Please, specify what is the time resolution of your model output.

Reply: We expanded our model description with respect to the processes governing the evolution of nitrate in PISCES (section 2.5, P8L14-P9L13). We included 5 equations: the full nitrate equation, the description of nitrate uptake by phytoplankton, the limitation terms and the full growth rate equation which controls PP. The time resolution of our model output was also added to the model description as well as the figure captions.

Subsection 3.1: The structure of this subsection is confusing, as it alternates results from the observations (paragraphs 1 and 3) and results from the model which actually in great part is a model evaluation. Please, move out the model evaluation from here and create a proper section that focuses on it, in order to refer to it also in the discussion when considering the limitations of the model. Also, please list first all the results obtained from the observations, and then those obtained from the model, without switching from one to the other in each paragraph.

Reply: We changed the structure of this section so that there is no longer an alternation between observations and model results. Also, we created a new section 3.1 dedicated to evaluating the mean physical and biogeochemical fields in the model. However, we kept some description of the simulated synoptic variability in section 3.2 (section 3.1 in the previous version) in order to be compared to the synoptic observations introduced there.

Page 11, line 7: "The variability of biogeochemical fields is similar to observations". Please, avoid using generic terms such as "similar".

Reply: We shortened this introduction sentence and it no longer contains the unspecific term "similar". The revised sentence is:

P16L12: "In the simulation, the upwelling structure also dominates the variability of the biogeochemical fields (Figs. 3d; 4i,j)."

Page 11, line 21-24: Please, remove this summary: these results are expected in any upwelling region, so it doesn't really add much information.

Reply: We shortened the paragraph concluding this section:

P16L27-29: "In brief, the near-surface cross-shore gradients of temperature, nitrate and chlorophyll are well represented in the simulation. In the following section we will see how both observed and modelled cold filaments give rise to along-shore variability by advection across these gradients."

Figure 3 and Figure 4: What do the model output sections represent? Is this still a single instance such as Figure 2 (April 5th 2017)? Or is this some longer term mean? Please, state this in the captions.

Also, how was the specific day for the model analysis and plots chosen?

Currently, some explanation is given in page 14 lines 31- 35, however some of the plots have already been introduced before this paragraph. Also, I would assume there are several events that may resemble the observations in the many years of model run, why was only a specific event chosen rather than using an ensemble of suitable events? Please, explain your rationale for the choice of day either in the captions or in the Methods.

Reply: We agree with the reviewer that information about the time average of the model output was missing in the captions and added it. However, after careful consideration we still think that the paragraph explaining why a quantitative comparison between the model and observed filaments is difficult (lines 31-35 in the former ms) needs to be part of section 3.2 (section 3.1 in the former ms) as it leads into the synoptic comparison of observations and model. This information would be misplaced in the new model evaluation (section 3.1), since that section focuses on 2-year averaged quantities. We therefore decided to keep the paragraph at its original place but reformulated and expanded our explanation. Some information about reasoning behind the choice of model output has also been included in the captions of figures already introduced before this paragraph. We now also include 2-year mean along-shore averaged sections for temperature and nitrate (Fig. 2c,e) in the manuscript, which are discussed in the model evaluation section (P12L25-P13L3).

Although comparing individual synoptic events is challenging and not sufficient as mentioned correctly by the reviewer it allows us to see how these structures are represented in the model, for example parameter gradients at frontal regions etc. Thus we think it is an important part of the model evaluation and only possible if high-resolution observations as presented in this study are at hand.

P18L33-P19L4: "The position and shape of simulated filaments is determined largely by the mesoscale eddy field, which evolves freely in the simulation and can therefore not be expected to correspond to the variability in the real ocean at any given time. The occurrence of major upwelling events and their effect on the variability of fronts and filaments, however, is closely related to the wind forcing of the model, which was derived from satellite-based, daily ASCAT

scatterometer winds. We therefore picked simulated filaments that were as close as possible in space and time to the observations, which were then taken to be representative of the area and season when the observations were carried out. The chosen filaments are comparable in scale to the observed cold filament, which had an offshore extent of 150 km - 200 km (Fig. 3a,b)."

Page 14, line 21: The paper provides a discussion of PP and how differently it relates to CHL in model and observations. Therefore, why is PP not plotted in Fig 3 and 4 if it's a variable of interest? Would it make sense to add it?

Reply: We decided to show PP in a separate table because of much fewer available observational profiles which don't lend themselves to plotting in 2D. Sampling the model output at comparable locations was more straightforward than vertical and horizontal interpolation of only a few observational data points, which would have required further assumptions. We now also decided to compute the vertical integral of the model simulations and include a comparison to satellite NPP in the model evaluation (section 3.1).

Page 14, line 31-32: Please, rephrase the first sentence as it's not good English. Page 14, line 33: Please rephrase here with "We therefore picked simulated filaments..."

Reply: We adapted the beginning of this paragraph (P14 lines 31-35 in the previous version) according to your suggestions and moved it before the model and data are compared. It now reads as follows:

P18L33-P19L4: "The position and shape of simulated filaments is determined largely by the mesoscale eddy field, which evolves freely in the simulation and can therefore not be expected to correspond to the variability in the real ocean at any given time. The occurrence of major upwelling events and their effect on the variability of fronts and filaments, however, is closely related to the wind forcing of the model, which was derived from satellite-based, daily ASCAT scatterometer winds. We therefore picked simulated filaments that were as close as possible in space and time to the observations, which were then taken to be representative of the area and season when the observations were carried out. The chosen filaments are comparable in scale to the observed cold filament, which had an offshore extent of 150 km - 200 km (Fig. 3a,b)."

Page 15, line 10: Please, substitute similar with similarly

Reply: The sentence has been corrected:

P19L14-15: "PP in the modelled filament is enhanced relative to the surrounding offshore waters, similarly to observations (Table 1)."

Page 15, line 17-27: This paragraph is not very useful and sounds like a repetition. It could be removed.

Reply: We think it is very helpful for the reader to get a short summary of the most important points but we shortened the paragraph:

P19L22-26: "In summary, the simulation exhibits upwelling filaments that are similar in lateral and horizontal scale and offshore extent to those observed. Our direct rate measurements indicate that PP in the modelled filaments is comparable to observations. Despite very low chlorophyll concentrations (< 0.1 mg m−3) in the observed filament, surface PP is by a factor 2 higher than at the upwelling front. This highlights the necessity of measuring PP in addition to chlorophyll for model validation to ensure a realistic representation of the underlying processes."

Page 15, line 29-30: I don't understand this first sentence. Since one can actually determine the simulated rate of nitrate uptake in the model, why should one "assume" something about it?

Reply: You are right that nitrate uptake is available as a diagnostic from our simulation. However, from the observations only total PP and nitrate concentration are available thus we cannot separate nitrate uptake from ammonium uptake. We commented on this aspect in the discussion (P27 lines 13-18). We rephrase this statement for clarity:

P19L28-34: "The model is able to reproduce realistic mixed-layer nitrate concentrations as well as mixed-layer PP rates offshore in the filaments, suggesting that the simulated rate of nitrate uptake (i.e. new production) is realistic as well (Figs. 3e,j; 4e,j; Table 1). However, it must be noted that our PP in situ estimates do not discriminate between new PP and regenerated PP resulting from ammonium uptake (see discussion section)."

Page 17, line 14-24: This section belongs to the Methods, not the Results.

Reply: We agree with your comment and have moved this paragraph to the methods (section 2.6, P10L9-19).

Page 17, line 24-26: Why should this implicit assumption be reasonable? Could you please provide some reason? Also, what is the definition of "subducted" - below what depth (this should be defined in the methods)?

Reply: A precise definition of subduction does not exist so we have to define our own. For our study, the subduction depth is defined in the methods (section 2.6, P10L14-16) as the base of the photic zone i.e. the depth of 0.1% surface PAR. Thus we consider a water parcel subducted once it leaves the photic zone. The

statement about the assumption is suppressed, as it was not necessary for our calculation and confusing. We thus rephrased as follows:

P21L7-P22L9: "Using the subduction ratio (Equation 7) defined in subsection 2.5, we estimate that 20 days after being upwelled 40.6% of the upwelled nitrate is subducted (Fig. 6f)."

Page 16, line 10: This initial sentence about the importance of SST remarks that it's crucial to include a good evaluation of the temperature gradient in the model.

Reply: We agree with the comment and modified the sentence:

P20L11-12: "The fate of upwelled floats is closely related to their change in temperature after upwelling, thus the correct representation of the temperature gradient in the model is crucial (Fig. 3a,b)"

Figure 7: The x-axis labels and ticks overlap in the subplots.

Reply: The overlapping x-axis tick labels have been removed (now Fig. 8 in revised manuscript).

Page 19, line 1-13: Wouldn't it be necessary to also discuss how the general model performance changes changing the resolution? What about the effects linked to the change in resolution of the forcing such as the wind stress, which is known to influence both upwelling and small scale flow? This paragraph compares two runs, but none of them was thoroughly evaluated.

Reply: In response to your comments we added a separate short section for model evaluation. The wind forcing is not likely to be a source of large differences between model resolutions, since the same relatively coarse data product (ASCAT at 1/4° resolution) is interpolated on both model grids. Only in a coupled ocean-atmosphere model simulation significant wind stress differences due to air-sea interaction at different scales would be expected. However, performing such a simulation (Ocean + Biogeochemistry + Atmosphere) at submesoscale resolution would be very expensive numerically and requires a lot of expertise for the atmospheric modelling part. This is however an interesting question that should be revisited in a future study.

Page19, line 20: Please add "is" in "during one season and is less..."

Reply: The sentence has been corrected, it now reads as follows:

P23L2-5: "Comparing the same virtual float experiment in different simulations illustrates well the relative changes in subduction and their biogeochemical impacts, but this Lagrangian approach is restricted to short integrations during

one season and is less suited to obtain estimates of absolute changes of the time-averaged model fields."

Page 19, line 31-32: Please rephrase better the sentence "Further offshore..."

Reply: This sentence has been rephrased:

P24L7-8: "Offshore of this negative change, an increase in nitrate (~ 1.5 μmol l^{-1}) is apparent around 100 m depth."

Page 20, line 1: Who are "they"?

Reply: The formulation was not clear and we rephrased the sentence as follows:

P24L10-11: "The horizontal patterns of nitrate change are largest in regions of increased eddy kinetic energy (not shown).

Page 20, line 2: Please substitute "a nitrate increase is found" with "nitrate increases"

Reply: We followed the reviewer's suggestion :

P24L11-12: "At a depth of 300 m to 500 m nitrate increases near the coast (~ 2 μmol l^{-1}), directly below the strong nitrate decrease in the top 200 m (~ −2.75 μmol l^{-1})."

Page 20, line 3-4: Why is this a "plausible explanation"? Too short and speculative, this needs to be expanded and explained better, possibly in the discussion.

Reply: We agree with the comment. We modified this part of the text following a comment of referee #1. It is now phrased as follows:

P24L12-P25L4: "A plausible explanation for this pattern is that due to increased offshore transport in the submesoscale simulation sinking organic matter sediments on deeper shelf areas, out of reach of the upwelling source waters. This would result in a downward redistribution of nitrate similar to the "nutrient leakage" described in Gruber et al. (2011). However, small differences in the alongshore mean circulation along the continental slope (not shown) may also modify the nitrate content of the water masses. Disentangling these processes is beyond the scope of the present work."

Page 23, line 7: Is this measurement from 1985 the only available measurement?

Reply: Direct PP measurements are still fairly limited compared to concentrations of biogeochemical parameters (eg. O2, CHL). To our knowledge this is the only measurement reported in the literature that was directly comparable to our measurements due to the location, dynamical setting and high horizontal resolution. We now also added PP rates from Fernández et al.

(2009) to the discussion, which were observed in a different season but geographically close to our study area (P27L6-10). From several other publications with PP measurements that are listed in Fernández et al. (2009), only integrated quantities are provided, which we did not calculate from our measurements. However, we calculated the vertically integrated mean PP from our simulations, to compare to the commonly used PP satellite products derived from ocean color (based on the Vertically Generalized Production Model (VGPM), Behrenfeld and Falkowski , 1997). We added some text and a reference on this in section 3.1 (P12L16-19). The corresponding sentences now read as follows:

P12L16-19: "Modelled PP in the 1/45° simulation exhibits a negative bias relative to PP estimates derived from ocean color (~ −37%). The spatial correlation of this modelled PP to the satellite estimate is high, and the standard deviation is only slightly underestimated in the simulation (r≈0.9, NSTD≈0.8), resulting in a good model fit (NRMSE≈0.45, Fig. 2a)."

P28L5-9: "The range of PP rates that were determined experimentally from incubations (Table 1) is very close to measurements by Dengler (1985) acquired during April-June 1976 in the upwelling center near 15° S (4 - 16 µmol C l^{-1} d^{-1}), increasing confidence in our results. In October 2005, Fernández et al. (2009) observed a similar range of PP rates in the top 25 m of the water column slightly north (3 - 16.5 µmol C l^{-1} d^{-1}; 11 - 12°S) and south (1 - 3.5 µmol C l^{-1} d^{-1}; 16 - 18° S) of our study area."

Ref.: Behrenfeld, M. J. & Falkowski, P. G. Photosynthetic rates derived from satellite-based chlorophyll concentration. Limnol. Oceanogr. 42, 1–20 (1997).

Ref.: Fernández, C., Farías, L. and Alcaman, M.E., 2009. Primary production and nitrogen regeneration processes in surface waters of the Peruvian upwelling system. *Progress in Oceanography*, 83(1-4), pp.159-168.

Page 20, line 5-15: This entire paragraph belongs to a model evaluation.

Reply: We assume here that the reviewer refers to the paragraph on page 23, lines 5-15, not page 20. We considered moving the paragraph to the newly incorporated model evaluation, but this was not logical in the structure of the paper since the section 3.1 is placed before the primary production measurements are introduced. We therefore kept the original position but split and reformulated the paragraph as follows:

P28L5-9: "The range of PP rates that were determined experimentally from incubations (Table 1) is very close to measurements by Dengler (1985) acquired during April-June 1976 in the upwelling center near 15° S (4 - 16 µmol C l^{-1} d^{-1}), increasing confidence in our results. In October 2005, Fernández et al. (2009)

observed a similar range of PP rates in the top 25 m of the water column slightly north (3 - 16.5 μmol C l^{-1} d^{-1}; 11 - 12°S) and south (1 - 3.5 μmol C l^{-1} d^{-1}; 16 - 18°S) of our study area."

P28L30-31: "Along-shore variability of PP in the simulation is closely related to chlorophyll concentrations, while the observed relationship of PP and chlorophyll is less clear (Table 1)."

P29L3-9: "Vertically, the modelled PP strictly decreases with larger depth corresponding to lower light levels, while in the observations subsurface maxima of PP are found offshore and at the upwelling front (Table 1). The subsurface chlorophyll maximum is too weak and diffuse in the simulations, which is consistent with this difference in the vertical distribution of PP. This could be partly related to dynamical bias in the simulations: Near-surface stratification at the base of the mixed-layer is by a factor of 2-3 lower in the model than in the observations, which likely results in a too diffuse offshore nutricline and contributes to the weak subsurface chlorophyll maximum. For the reasons mentioned above, subsurface PP in the offshore waters is likely too low in our simulations."

Introduction/Discussion: Please, include the following relevant literature and discuss how it compares to your findings

FILAMENTS STRUCTURE

- Bettencourt, J. H., Rossi, V., Hernández‐García, E., Marta‐Almeida, M., and López, C. (2017), Characterization of the structure and cross‐shore transportpropertiesofacoastalupwellingfilamentusingthree‐dimensionalfinite‐size Lyapunov exponents, J. Geophys. Res. Oceans, 122, 7433– 7448, doi:10.1002/2017JC012700.

IMPACT OF MODEL RESOLUTION ON VERTICAL FLUXES

- Zhong, Y., and Bracco, A. (2013), Submesoscale impacts on horizontal and vertical transport in the Gulf of Mexico, J. Geophys. Res. Oceans, 118, 5651– 5668, doi:10.1002/jgrc.20402.

- Zhong, Y., Bracco, A., Tian, J. et al. Observed and simulated submesoscale vertical pump of an anticyclonic eddy in the South China Sea. Sci Rep 7, 44011 (2017). https://doi.org/10.1038/srep44011

SUBDUCTION BY FRONTS

- Stukel, M.R., Song, H., Goericke, R. and Miller, A.J. (2018), The role of subduction and gravitational sinking in particle export, carbon sequestration, and the remineraliza- tion length scale in the California Current Ecosystem. Limnol. Oceanogr., 63: 363-383. doi:10.1002/lno.10636

- Michael R. Stukel, Lihini I. Aluwihare, Katherine A. Barbeau, Alexander M. Chekalyuk, Ralf Goericke, Arthur J. Miller, Mark D. Ohman, Angel Ruacho, Hajoon Song, Brandon M. Stephens, Michael R. Landry Proceedings of the National Academy of Sciences Feb 2017, 114 (6) 1252-1257; DOI: 10.1073/pnas.1609435114

Reply: We have added some of the literature you suggested to the discussion. However, because the discussion is already quite long and we wanted to avoid compromising the readability of our paper too much, we selected only the most relevant references.

P29L23-26: "More generally, Zhong and Bracco (2013) and Zhong et al. (2017) find that submesoscale frontal processes are important for the vertical tracer transports near the surface and that vertical dispersion of Lagrangian particles strongly increases with increasing horizontal model resolution, which is also in agreement with the results of this study."

P29L30-31: "Subduction at fronts has previously been shown in observations to be as important for organic matter export below the photic zone as gravitational sinking (Stukel et al., 2017)."

The fate of upwelled nitrate off Peru shaped by submesoscale filaments and fronts

Jaard Hauschildt[1], Soeren Thomsen[1,2], Vincent Echevin[2], Andreas Oschlies[1], Yonss S. José[1], Gerd Krahmann[1], Laura A. Bristow[3,4], and Gaute Lavik[3]

[1]GEOMAR Helmholtz Centre for Ocean Research Kiel, Kiel, Germany
[2]Laboratoire d'Océanographie et du Climat, Expérimentations et Approches Numériques (LOCEAN), Institut de Recherche pour le Développement (IRD), Institut Pierre-Simon Laplace (IPSL), Université Pierre et Marie Curie (UPMC), Paris, France
[3]Max Planck Institute for Marine Microbiology (MPI), Bremen, Germany
[4]Department of Biology / Nordcee, University of Southern Denmark (SDU), Odense, Denmark

Correspondence: Jaard Hauschildt (jhauschildt@geomar.de)

Abstract. Filaments and fronts play a crucial role for a net offshore and downward nutrient transport in Eastern Boundary Upwelling Regions (EBUS) and thereby reduce primary production. Often studies are either based on observations or model simulations but seldom both approaches are combined quantitatively to assess the importance of filaments for primary production and nutrient transport. Here we combine targeted interdisciplinary shipboard observations of a cold filament off Peru with submesoscale-permitting (1/45°) coupled physical (CROCO) and biogeochemical (PISCES) model simulations to (i) evaluate the model simulations in detail, including the timescales of biogeochemical modification of the newly upwelled water and (ii) quantify the net effect of submesoscale fronts and filaments on primary production of the Peruvian upwelling system. The observed filament contains relatively cold, fresh and nutrient-rich waters originating in the coastal upwelling. Enhanced nitrate concentrations and offshore velocities of up to $0.5 \, \text{m s}^{-1}$ within the filament suggest an offshore transport of nutrients. **Surface chlorophyll in the filament is a factor 4 lower than at the upwelling front while surface primary production is a factor 2 higher.** The simulation exhibits filaments that are similar in horizontal and vertical scale compared to the observed filament. Nitrate concentrations and primary production within filaments in the model are comparable to observations as well, justifying further analysis of nitrate uptake and subduction using the model. Virtual Lagrangian floats were released in the subsurface waters along the shelf and biogeochemical variables tracked along the trajectories of floats upwelled near the coast. In the submesoscale-permitting (1/45°) simulation 43.0 % of upwelled floats and 40.6 % of upwelled nitrate is subducted within 20 days after upwelling, which corresponds to an increase of nitrate subduction compared to a mesoscale-resolving (1/9°) simulation by 13.9 %. **Taking model biases into account we give a best estimate for subduction of upwelled nitrate off Peru between 30.5 - 40.6 %. Our results suggest** that submesoscale processes further reduce primary production by amplifying the downward and offshore export of nutrients found in previous mesoscale studies, which are thus likely to underestimate the reduction in primary production due to eddy-fluxes. Moreover, this downward and offshore transport could also enhance the export of fresh organic matter below the photic zone and thereby potentially stimulate microbial activity in the upper offshore oxygen minimum zone.

1 Introduction

The eastern margins of the subtropical oceans are characterized by upwelling of cold and nutrient-rich subsurface waters, caused by persistent along-shore winds that drive an offshore Ekman transport. The nutrients supplied to the sunlit surface ocean subsequently fuel high phytoplankton growth which supports a rich ecosystem (Pennington et al., 2006). These Eastern Boundary Upwelling Systems (EBUS) are found in all major ocean basins and named after the Canary, Benguela, California, and Peru-Chile current systems. The Peru-Chile upwelling system (PCUS) is the most productive EBUS in the global ocean, accounting for 10 % of the global fish catch while occupying only 0.1 % of the ocean surface (Chavez et al., 2008). The Peru upwelling ecosystem and the fisheries that depend on it thus have immense economical importance for the local population. **Furthermore, the high productivity and export of organic matter and its subsequent remineralization at depth result in high oxygen consumption (Kalvelage et al., 2015; Loginova et al., 2019). In combination with poor ventilation by sluggish currents this leads to the presence of the shallowest and most intense oxygen minimum zone (OMZ) in the global ocean (Wyrtki, 1962; Paulmier et al., 2006; Karstensen et al., 2008; Stramma et al., 2010).** Global relevance is given to EBUS by their role as natural sources of greenhouse gases to the atmosphere such as N_2O (Friederich et al., 2008; Arévalo-Martínez et al., 2015) and CO_2 (Chavez et al., 2007; Gruber, 2015; Köhn et al., 2017; Brady et al., 2019).

The circulation in the Peru-Chile current system is characterized by opposing surface and subsurface along-shore currents: the Peru Coastal Current flows equatorward near the surface (Penven et al., 2005). The subsurface Peru-Chile Undercurrent (PCUC) flows poleward with a velocity of 10 - 15 cm s^{-1} at 100 m - 150 m depth along the shelf (Wyrtki, 1963, 1967; Brink, 1983; Huyer et al., 1991; Strub et al., 1998; Chaigneau et al., 2013), supplying the nutrient-rich source waters of the coastal upwelling. Between 11 °S - 16 °S, southward velocities of 10 - 15 cm s^{-1} are observed at only 25 m depth, related to a near-surfacing of the PCUC (Chaigneau et al., 2013; Pietri et al., 2014).

Mesoscale eddies have in the past been assumed to generally enhance biological productivity in the open ocean by either exposing nutrient-rich subsurface water to the well-lit euphotic zone or by lateral advection of nutrients (Falkowski et al., 1991; McGillicuddy et al., 1998; Oschlies, 2002). Conversely, in the highly productive EBUS eddies and filaments have been shown to decrease productivity by exporting nutrients and organic matter offshore and downward below the euphotic zone (Rossi et al., 2008, 2009; Lathuilière et al., 2010; Gruber et al., 2011; Nagai et al., 2015). Such features are ubiquitous in the PCUS (Penven et al., 2005; Colas et al., 2012; Thomsen et al., 2016a, b; Pietri et al., 2013; McWilliams et al., 2009). As the upwelling front meanders and eventually becomes unstable, an ageostrophic secondary circulation develops in order to restore geostrophic balance (Thomas et al., 2008; McWilliams et al., 2009, 2015). This ageostrophic flow field can drive large vertical velocities and thus impact the physical-biogeochemical coupling by modifying vertical and lateral transports of nutrients and organic matter (Lapeyre and Klein, 2006; Lévy et al., 2012; Mahadevan, 2015). The downward fluxes can be understood as subduction of surface water along isopycnals out of the mixed-layer.

Previous studies have attempted to quantify the fluxes of biogeochemical tracers related to eddies and filaments in EBUS using biogeochemical models of various complexity (e.g. Nagai et al., 2015 in the California EBUS; Frenger et al., 2018; Montes et al., 2014; Bettencourt et al., 2015; José et al., 2017 in the PCUS; Lovecchio et al., 2018 in the

Canary EBUS, Schmidt and Eggert, 2016 in the Benguela EBUS). However, most of these studies are purely based on models and comparison to observations has proven difficult, due to the difficulties of observing vertical velocities. Also, iron is known to play a role in limiting primary production in the PCUS (Hutchins et al., 2002; Bruland et al., 2005; Browning et al., 2018) which previous model studies have not addressed with respect to eddy-fluxes of biogeochemical tracers. Regional simulations are often mainly validated using surface chlorophyll maps derived from ocean color, which does not allow to assess the underlying physical (e.g. subduction) and biogeochemical processes (e.g. primary production, hereafter PP). **For instance, if the time scale of nitrate uptake by PP was shorter than that of subduction, mainly organic matter produced in the surface layer would be subducted. If it were longer, mainly nitrate would be subducted.** When attempting to quantify the effect of subduction on biogeochemistry using models, we therefore need to ensure that the timescales of PP and subduction are realistic. **Dedicated studies combining multi-disciplinary observations with modelling efforts at meso- and submesoscale are key to advance our understanding of complex physical-biogeochemical interactions (Oschlies et al., 2018).** Evaluating the models at these scales allows to gain trust in the simulation of submesoscale processes and assess the associated uncertainties and possible systematic biases.

Furthermore, the degree to which dynamical processes of a certain scale are represented in a simulation depends on the effective horizontal resolution of the numerical model (Capet et al., 2008a; Soufflet et al., 2016). So far, coupled physical-biogeochemical model simulations focusing on eddy-fluxes of biogeochemical tracers (e.g. Nagai et al., 2015 for the California EBUS) were limited to a horizontal resolution of ~ 5 km in mid-latitudes, which is not sufficient to represent submesoscale dynamics as the effective resolution is much lower due to strong kinetic energy dissipation at the smallest resolved scales (Soufflet et al., 2016). Various purely physical model simulations (Capet et al., 2008b; Colas et al., 2012) and idealised biogeo-chemical simulations (Lathuilière et al., 2010) suggest that an increase in the horizontal resolution leads to further enhancement of horizontal and vertical fluxes.

In this study, we will focus on filaments and fronts which constitute the upper end of the submesoscale variability spectrum with length scales of $\mathcal{O}(1 \text{-} 10)$ km (McWilliams, 2016). To this aim we will simulate the PCUS dynamics using a coupled physical-biogeochemical model of 2.5 km resolution. A quantification of the net effect of filaments and submesoscale frontal processes on the offshore and downward nutrient transport and **PP** off Peru is missing so far. Therefore, we will address the following questions:

1. What is the amount of nitrate subduction and how does it impact PP?

2. What is the impact of horizontal model resolution on subduction and PP?

To address these questions, we will evaluate the model based on physical and biogeochemical observations of a cold filament. To assess the timescale of phytoplankton growth in our model, we will compare PP and nutrient concentrations in a modelled filament with observational data. Then, we will quantify how much of the upwelled nitrate off Peru is subducted below the euphotic zone and not taken up by biology.

This paper is structured as follows: **In section 2 the filament survey, the coupled physical-biogeochemical model and all other data sources as well as analysis methods are described. In section 3.1 the model performance with respect**

to the relevant physical and biogeochemical quantities and their horizontal variability is evaluated. In section 3.2 and section 3.3 the mean horizontal variability of the upwelling structure and cold filaments are characterized in detail both in observations and model simulations. In section 3.4 the simulation is used to analyse pathways and timescales of nitrate export, subduction and uptake and compare them to estimates from observations. In section 3.5 the effect of submesoscale-permitting vs. mesoscale model resolution on the mean biogeochemical fields is analysed. Finally, the results are discussed in the context of existing literature in section 4, which also includes a detailed discussion of the limitations of our approach. Concluding remarks follow in section 5.

2 Data and methods

2.1 Filament survey

A survey designed to investigate the biophysical coupling at a cold filament near 14 °S off the coast of Peru was carried out on April 12-17, 2017 using an adaptive sampling strategy guided by real-time satellite images. The field work was conducted during *R/V Meteor* cruise M136 which started on April 11 and ended on April 29, 2017 in Callao, Peru (Dengler and Sommer, 2017; Lüdke et al., 2019). The measurements were carried out as part of the "SFB754 - Climate-Biogeochemistry Interactions in the Tropical Ocean" project. The cruise track during the survey consisted of five transects (Fig. 1a). The first transect (CROSS) mapped the upwelling region in cross-shore direction with conductivity, temperature and depth (CTD) measurements including biogeochemical parameters (O_2 , NO_3^-, NO_2^-, NH_4^+) determined from water samples. On subsequent along-shore transects, a cold filament present ~ 100 km southeast of transect CROSS was crossed by *R/V Meteor* four times in a zigzag pattern: Twice with high-resolution physical underway CTD measurements heading in southeast direction (PHY, PHY2) and two more times with station-based lowered CTD measurements including biogeochemical parameters heading in northwest direction (BIO, BIO2). A dense sampling strategy with 8 - 10 km horizontal spacing between stations and 5 - 10 m vertical spacing between samples was applied for the biogeochemical transects. The physical underway transects (PHY, PHY2) were completed overnight in under 8 hours sampling with a horizontal spacing of under 1 km, similar to the resolution of the binned ADCP data. This physical data thus closely represents a synoptic view of the surface ocean. Sampling on the biogeochemical transects (BIO, BIO2) was done during daytime following each physical transect. Wind speed and direction on *R/V Meteor* were measured at 35.5 m height with a temporal resolution of one minute and corrected to 10 m height following Smith (1988), similar to the procedure used by Köhn et al. (2017).

2.2 Oceanographic biophysical measurements

Hydrographic data was obtained from lowered conductivity, temperature and pressure (CTD) measurements using SeaBird SBE 9-plus CTD system equipped with two sets of pumped sensors. Water samples for oxygen, nutrients and salinity were taken using 24 Niskin bottles (10 l) mounted on a General Oceanics rosette. Salinity samples were analyzed on board with a Guildline Autosal 8 model 8400B salinometer to calibrate conductivity measurements to practical salinity (PSS-78) with an uncertainty

4

of 0.003 g kg^{-1}. Practical salinity was converted to absolute salinity (TEOS-10) using routines of the Gibbs Seawater toolbox (https://github.com/TEOS-10/GSW-Python). The CTD was also equipped with an oxygen sensor and a WET Labs (USA) fluorometer. The oxygen sensor was calibrated to an accuracy of 1.5 μmol using Winkler titration. As Winkler titration is not reliable in the core of the OMZ and results in too high values (Revsbech et al., 2009; Kalvelage et al., 2013; Thomsen et al., 2016b), a concentration of 0 μmol l^{-1} was assumed in the core of the OMZ and the profiles corrected accordingly following Langdon (2010). To determine chlorophyll-a concentrations from the measured chlorophyll fluorescence, the original factory calibration provided by the sensor manufacturer WET Labs (USA) was used. For more details on calibration of chlorophyll fluorescence measurements, the reader is referred to Loginova et al. (2016). Underway subsurface temperature and salinity were measured using a Teledyne Oceanscience (Poway, USA) RapidCAST system acquiring profiles of the upper 70 m of the water column every 2 minutes resulting in a horizontal resolution of 790 ± 240 m depending on the vessel speed. Subsurface current velocities on *R/V Meteor* were recorded by a vessel-mounted Acoustic Doppler Current Profiler (vmADCP). The system used was a Teledyne RD Instruments OceanSurveyor 75kHz ADCP capable of reaching a maximum depth of ~700m. The shallowest velocity measurements were acquired in a bin centered 18 m below the sea-surface. During the filament crossing, the vessel speed was kept nearly constant at ~5 m s^{-1} to obtain high-quality velocity measurements with a vertical resolution of 8 m and a horizontal resolution of 290 ± 26 m which was subsequently averaged in 1 km bins. Nutrient concentrations were determined onboard by a QuAAtro autoanalyzer (SEAL Analytical, Southampton, UK) using standard photometric methods (Grasshoff et al., 1983).

During M136 a self-contained ultraviolet SUNA nitrate sensor manufactured by Sea-Bird Scientific was attached to the CTD/Rosette system similar to Alkire et al. (2010). SUNA sensors determine the concentration of nitrate by measuring the absorption of UV light over a fixed path length. The SUNA data has been reprocessed with the concurrent CTD pressure, temperature, and salinity (for bromide absorption) data to eliminate their effects on the absorption and the resulting nitrate concentrations (Sakamoto et al., 2009, 2017). The resulting SUNA nitrate concentrations have been extracted for the times at which bottles were closed on the watersampler. These concentrations have then been compared to the nitrate and nitrite concentrations measured with the Autoanalyzer. SUNA nitrate values correlated highly with the Autoanalyzer values (r-squared 0.9972, with the 10% most deviating samples removed). SUNA values were also compared to the combined Autoanalyzer concentrations of nitrate and nitrite but the resulting correlation was somewhat weaker (r-squared 0.9964, with the 10% most deviating samples removed). The SUNA measurements were thus corrected to match the nitrate (NO_3) concentration by applying the following correction term where $NO_{3,\,old}$ is the original measurement and $NO_{3,\,new}$ is the final corrected value: $NO_{3,\,new} = 1.2813 + 1.0576 \times NO_{3,\,old}$. We applied this calibration to all SUNA nitrate concentrations.

2.3 Incubations

Seawater samples were filled into 2 L polycarbonate bottles, and were stored in the dark until tracer additions were made, which was always within 2 hours of collection. Following the method outlined in Großkopf et al. (2012), incubations were started with the addition of sodium bicarbonate (NaH$_{13}$CO$_3$; > 98 atom%, Sigma Aldrich) to yield an enrichment of approximately

3.2 atom% final. At each depth sampled, three bottles received a ^{13}C addition, and a fourth bottle received no ^{13}C and acted as an untreated control allowing the natural abundance ^{13}C to be determined at each depth. All bottles were placed into on-deck incubators with surface seawater flow-through and shaded with 20, 10 or 1% surface irradiance (Lee Filters, Seattle, WA, USA), depending on the sampling depth. Incubations were terminated after 24 hours by filtration onto 25mm pre-combusted

5   (450°C, 4 h) GF/F filters (Whatman), which were dried onboard (50°C, 12 h) and stored at room temperature until analysis. Prior to analysis GF/F filters were acidified over fuming HCl overnight in a dessicator, dried and pelletized in tin cups. Samples were analyzed for particulate organic carbon and isotopic composition using continuous flow isotope ratio mass spectrometry coupled to an elemental analyzer. PP rates were calculated from the incorporation of ^{13}C into biomass as described in Großkopf et al. (2012).

10   ## 2.4 Data products

To guide the shipboard measurements and put them into a regional context MODIS (Moderate Resolution Imaging Spectroradiometer) Level 2 along-track sea-surface temperature (SST) and chlorophyll-*a* products with an approximate resolution of 1 km from the TERRA and AQUA satellites were used (https://oceandata.sci.gsfc.nasa.gov/). We restricted our analysis to daylight images of SST and used the cloud mask based on ocean color because of obvious deficiencies of the

15   cloud mask based on infrared SST data alone. SST data from AVHRR (Advanced Very High Resolution Radiometer) at 25 km resolution was downloaded from NOAA (ftp://eclipse.ncdc.noaa.gov/pub/OI-daily-v2/NetCDF/). **For evaluating the model performance with respect to PP, we used estimates of ocean Net Primary Production (NPP) which were derived from both MODIS and SeaWIFS chlorophyll-*a* using the Vertically Generalized Production Model (VGPM, Behrenfeld and Falkowski, 1997, http://sites.science.oregonstate.edu/ocean.productivity/). A global mixed-layer depth**

20   **(MLD) climatology with $2° \times 2°$ resolution based on a $0.2°$C temperature criterion was provided by IFREMER (http://www.ifremer.fr/cerweb/deboyer/mld/Surface_Mixed_Layer_Depth.php). Annual mean temperature and nitrate fields for model evaluation were provided at $1/2°$ resolution by the CARS climatology (CSIRO Atlas of Regional Seas, Ridgway et al., 2002, http://www.marine.csiro.au/atlas/). Annual mean gridded chlorophyll-*a* products from the MODIS and SeaWIFS satellite-based instruments were downloaded from NOAA (https://oceandata.sci.gsfc.nasa.gov/).**

25   ## 2.5 Coupled Physical-Biogeochemical Model (CROCO/PISCES)

We employed CROCO (Coastal and Regional Ocean Community model) to study the circulation in the PCUS at submesoscale-permitting resolution. CROCO is a free-surface, terrain-following coordinate ocean modeling system built upon ROMS_AGRIF (Penven et al., 2006; Shchepetkin and McWilliams, 2009) and a non-hydrostatic kernel (not used in this study). CROCO solves the Primitive Equations using the Boussinesq approximation and a hydrostatic vertical momentum balance. **The nonlocal K-**

30   **Profile Parameterization (KPP) scheme is used to handle unresolved processes related to vertical mixing.** For a complete description of the model numerical schemes the reader can refer to Shchepetkin and Mcwilliams (2005). The code used in the present study is the CROCO v1.0 version, which is very similar to ROMS_AGRIF version v3.1.
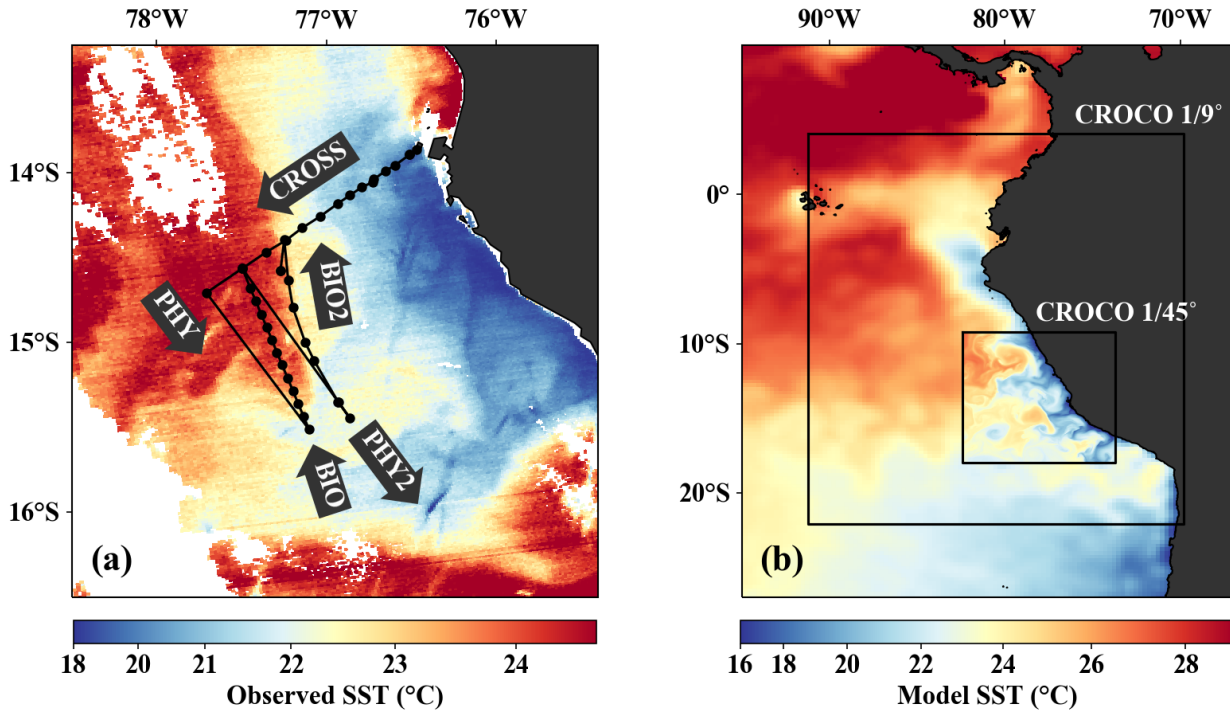
Figure 1. (a) Observed SST (MODIS) on April 14, 2017 with cruise track and section names superimposed (b) Model SST on April 14, 2017 in the coarse- (1/9 °) and high-resolution (1/45 °) CROCO simulations superimposed on AVHRR satellite SST. Black rectangles indicate the respective model domains.

The model was configured as a nested set of two spatial domains (Fig. 1b) using an offline, one-way embedding procedure (Mason et al., 2010). The outer domain has a resolution 1/9 ° over a region of 2207 km in zonal direction by 2911 km in meridional direction (24.4 ° x 26.2 °), and the inner domain has a resolution of 1/45 ° over a region of 918 km in zonal direction by 973 km in meridional direction (8.69 ° x 8.76 °). **Since the Peruvian upwelling system is located relatively close to the equator, the Rossby radius is about 70 km in our study area (Chelton et al., 1998), an order of magnitude larger than our model resolution (~ 2.5 km). The Rossby radius represents effectively the limit of mesoscale dynamics and we can thus consider our model submesoscale-permitting, as it resolves the upper range of the submesoscale variability spectrum.** There are 32 sigma-levels and the vertical resolution varies with water depth. Here we focus on the upper 200 m of the water column where the vertical resolution near the surface is 1 - 2 m / 5 m on the shelf / offshore. The model topography was derived from the GEBCO (General Bathymetric Chart of the Oceans, http://www.gebco.net) product, interpolated onto the model grid and smoothed to reduce pressure gradient errors.

The lateral open boundary conditions of the outer domain for temperature, salinity, velocities and sea-level were provided at 1/12 ° resolution by the MERCATOR PSY4V2 model (Lellouche et al., 2018) which assimilated in-situ data transmitted from *R/V Meteor* during the research cruises M135 (large scale mapping off the OMZ, https://doi.pangaea.de/10.1594/PANGAEA.

890441) and M136 (https://doi.pangaea.de/10.1594/PANGAEA.892564) and from ARGO floats (http://www.argo.ucsd.edu/), as well as satellite SST and sea-level measurements. No assimilation or "nudging" was done inside the model domain except for a restoring term on the surface heat flux. The net surface heat flux Q is given by the COADS (Worley et al., 2005) climatology relaxed to AVHRR (Advanced Very High Resolution Radiometer; ftp://eclipse.ncdc.noaa.gov/pub/OI-daily-v2/NetCDF/) daily SST according to

$$Q = Q_{\text{COADS}} - \frac{dQ}{dT} \cdot (\text{SST}_{\text{CROCO}} - \text{SST}_{\text{AVHRR}}) \tag{1}$$

where $\frac{dQ}{dT}$ represents the additional heat flux that is imposed per degree of temperature difference between model SST and observed SST. This heat flux correction is a function of atmospheric parameters and assumes values of $30\text{-}35$ W/m^2/$^\circ$C (Barnier et al., 1995). The model was forced with surface wind stress derived from the daily level-2 wind product provided by the ASCAT scatterometer (https://podaac.jpl.nasa.gov/dataset/ASCATB-L2-25km).

The CROCO model was coupled to the PISCES (Pelagic Interaction Scheme for Carbon and Ecosystem Studies) biogeo-chemical model which simulates the biogeochemical cycles of carbon and the main nutrients (P, N, Si, Fe). It includes two phytoplankton compartments (nanophytoplankton and diatoms), two zooplankton size classes (microzooplankton and meso-zooplankton), two detritus classes and a description of the carbonate chemistry. **A detailed model description is given in Aumont et al. (2015), in the following we will outline only the equations that are relevant for our analysis of the local temporal nitrate changes. The evolution of nitrate in PISCES is determined by equation (2), with the right-hand side terms representing nitrate increase due to nitrification and nitrate loss due to small phytoplankton growth, large phytoplankton growth and denitrification (we omitted the physical transport and mixing terms):**

$$\frac{\partial \text{NO}_3}{\partial t} = \text{Nitrif} - \mu^P_{\text{NO}_3} P - \mu^D_{\text{NO}_3} D - \text{Denitrif} \tag{2}$$

The nitrate uptake rate of small phytoplankton $\mu^P_{\text{NO}_3}$ is defined by equation (3) as follows:

$$\mu^P_{\text{NO}_3} = \mu^P \frac{L^P_{\text{NO}_3}}{L^P_{\text{NO}_3} + L^P_{\text{NH}_4}} \tag{3}$$

The limitation term for nitrate $L^P_{\text{NO}_3}$ is described by equation (4):

$$L^P_{\text{NO}_3} = \frac{K^P_{\text{NH}_4} \text{NO}_3}{K^P_{\text{NO}_3} K^P_{\text{NH}_4} + K^P_{\text{NH}_4} \text{NO}_3 + K^P_{\text{NO}_3} \text{NH}_4} \tag{4}$$

The limitation term for ammonium $L^P_{\text{NH}_4}$ is similar to equation (4) but with the product of ammonium concentration NH_4 and half-saturation constant $K^P_{\text{NO}_3}$ in the numerator. The half-saturation constants for nitrate $K^P_{\text{NO}_3}$ and for ammonium $K^P_{\text{NH}_4}$ set the concentrations at which the limiting effect of each nutrient would result in half the maximum growth rate. The growth rate for small Phytoplankton μ^P is described by equation (5),

$$\mu^P = \mu^0_{\max} f_1(T) f_2(L_{\text{day}}, z_{\text{mxl}}) \left(1 - \exp\left(\frac{-\alpha^P \theta^{\text{Chl},P} \text{PAR}^P}{L_{\text{day}} \mu^0_{\max} f_1(T) L^P_{\text{lim}}} \right) \right) L^P_{\text{lim}} \tag{5}$$

where μ_{max}^0 is the maximum growth rate at $0°$C and f_1 is a function describing the dependence on the temperature T of the growth rate. The function f_2 introduces additional dependencies of the growth rate on the length of day L_{day} and the mixed layer depth z_{mxl} in case it exceeds the euphotic zone. The term inside the parentheses is defined so that it increases exponentially with the amount of absorbed light given by the product of a constant parameter α^P, the variable chlorophyll to carbon ratio $\theta^{\text{Chl},P}$ and the photosynthetically available radiation PAR^P. The total nutrient limitation term L_{lim}^P is defined in such a way (Equation 6) that the nutrient with the smallest individual limitation term (i.e. the smallest concentration relative to its half-saturation constant) is taken to be the limiting nutrient and controls phytoplankton growth. Since phytoplankton can use both nitrate and ammonium as a nitrogen source, the individual limitation terms for these nutrients are added before calculating the total nutrient limitation term.

$$L_{\text{lim}}^P = \min\left(L_{\text{PO}_4}^P, L_{\text{NO}_3}^P + L_{\text{NH}_4}^P, L_{\text{Fe}}^P\right) \tag{6}$$

The equations for the nitrate uptake rate of large phytoplankton $\mu_{\text{NO}_3}^D$ (see equation 2) have an identical structure to equations 3-6 and are therefore omitted here. Primary production is proportional to the sum of the small phytoplankton biomass P and large phytoplankton biomass D, multiplied by their respective growth rates μ^P and μ^D.

The open boundary conditions for oxygen, nitrate, phosphate and silicate were provided at $1/2°$ resolution by the CARS climatology (CSIRO Atlas of Regional Seas, Ridgway et al., 2002) as the sum of an annual mean and both annual and semi-annual cycles. For the variables not available from data climatologies (iron, dissolved organic & inorganic carbon, total alkalinity), a climatology derived from model output of a global NEMO-PISCES simulation at $2°$ resolution was used (Aumont et al., 2015). After a spinup of 14 years for the $1/9°$ simulation, the $1/9°$ and $1/45°$ simulations were started from this model state and run from January 2013 until April 2017. Only model data from March 2014 onwards has been used in the analysis to allow for an additional spinup of the submesoscale dynamics in the $1/45°$ nest. **The model output frequency was set to 1 day for the $1/45°$ simulation and 3 days for the $1/9°$ simulation, except for the Lagrangian analysis where we generated additional output at 4-hour frequency from both simulations to allow for a more precise offline calculation of the float trajectories and ensure that the results are comparable.**

2.6 Virtual Lagrangian float experiment

To study the temporal evolution of biogeochemical properties in the upwelled water, an ensemble of 20 float experiments was conducted. The ensemble consist of 5 experiments each performed in April of the years 2014 - 2017 and initialised on day 1, 6, 11, 16 and 21. For each of these experiments, 250.000 virtual Lagrangian floats were advected by the 4 h average model flow field for 35 days using the ROMS offline tool (Capet et al., 2004; Carr et al., 2008). Virtual floats were released between the coast and ~ 250 km offshore over the upper 150 m and biogeochemical variables were tracked along float trajectories. Following Thomsen et al. (2016a) we subsampled the trajectories of all floats that (1) are in the euphotic zone at a given time, (2) were below the euphotic zone for at least 1 day before that and at the time of release, (3) have a density higher than $25\,\text{kg}\,\text{m}^{-3}$ and (4) are located between $13°$S and $16°$S which we then consider as upwelled. The euphotic zone is defined as

the upper layer of the ocean where photosynthetically active radiation is > 1% of its surface value. The duration of 1 day was chosen somewhat arbitrarily to exclude floats that have their source at the surface and are simply subject to relatively short, alternating vertical motions while they enter the upwelling patch. This is justified as the upwelling implies a source at the subsurface and the results are not sensitive to this parameter choice. The density criterion (3) is imposed to restrict our analysis to the trajectories that surface inshore of the upwelling front, where the densest isopycnals outcrop. The regional criterion (4) ensures that the upwelled floats originate close to the center of the model domain and will only rarely reach the open boundaries during the experiment. It also serves the purpose of maintaining comparability with the observational data that was collected in this region.

To analyse the fate of upwelled nitrate in more detail, we used the subsampled float trajectories to compute the fraction of upwelled nitrate that is subducted. We computed a "subduction ratio" as follows:

$$\text{ratio} = \frac{\sum_{i=1}^{N_{\text{subducted}}} \text{NO}_{3\,i,t_{20}}}{\sum_{i=1}^{N_{\text{upwelled}}} \text{NO}_{3\,i,t_{0}}} \tag{7}$$

where N_{upwelled} is the total number of upwelled floats, $N_{\text{subducted}}$ is the total number of subducted floats, $\text{NO}_{3\,t_0}$ is the nitrate concentration of each float at the time of upwelling and $\text{NO}_{3\,t_{20}}$ is nitrate concentration of each float 20 days after upwelling. We first save the nitrate concentration for each individual float at the time of upwelling. If a float is below the photic zone - defined as 0.1% surface intensity PAR - 20 days after upwelling, we consider this float subducted and also save the nitrate concentration at this time. The sum of the nitrate concentration over the subducted floats divided by the sum of the nitrate concentration over all upwelled floats yields the nitrate subduction ratio. Using this ratio we can account for the reduction in nitrate during the time period that the subducted floats stay in the photic zone. A timescale of 20 days was chosen because the number of upwelled floats below the photic zone appears to **have stabilized** after this time (Fig. 6f).

3 Results

3.1 Model evaluation

Before using the submesoscale-permitting simulation to analyse the process of nitrate subduction in the Peruvian up-welling, we verify that the simulation realistically captures the relevant physical and biogeochemical dynamics. The model evaluation focuses here on time-averaged mean quantities and their horizontal variability as a detailed comparison of the simulation to observations on synoptic scales follows in the next subsections. The 2-year averaging period (2015-2016) is chosen to allow for sufficient spin-up of small-scale dynamics in the 1/45° simulation, which was initialised on January 1, 2013.

The model fit of the most relevant physical and biogeochemical variables to observations is summarised in Taylor diagrams for both the 1/45° and 1/9° simulations (Fig. 2a,b). The simulated SST shows only a small negative bias (~ −3%) relative to satellite observations for both simulations. The spatial patterns of simulated and observed mean SST are
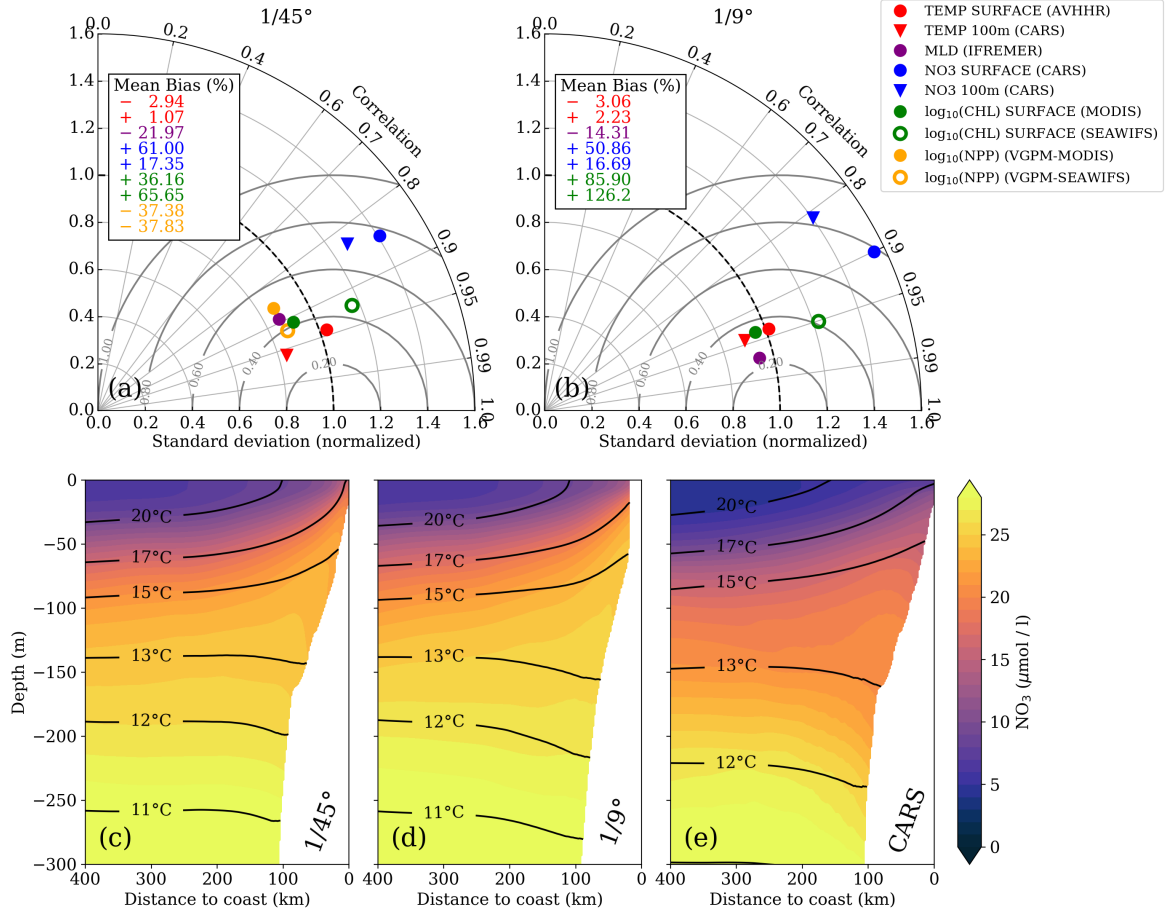
Figure 2. Taylor diagrams for (a) 1/45° and (b) 1/9° simulations, respectively. The statistics were computed from horizontal mean fields (see Fig. S1) and therefore represent their spatial variability. Due to the strongly skewed distributions of chlorophyll-a and PP these variables were logarithmized prior to computing correlation and standard deviation to approximate normally distributed variables, while the mean bias was calculated using the original values. Grey concentric circles centred around unity normalised standard deviation and correlation indicate the normalised root mean square error (NRMSE). The analysis for the 1/9° simulation was restricted to the extent of the 1/45° domain to facilitate direct comparison. Primary production rates were not saved for the 1/9° simulation and could therefore not be evaluated. (c-e) Along-shore averaged sections of mean nitrate concentrations with temperature contours superimposed for (c) 1/45° simulation, (d) 1/9° simulation and (e) CARS climatology. The CARS climatology was interpolated onto the 1/45° model grid before computing the along-shore average.

also highly correlated (r=0.95) and their standard deviations are almost identical, resulting in a normalized standard deviation of about unity (NSTD≈1). This is expected since the same SST observations are also used to calculate the restoring term on the surface heat flux at runtime of the model, effectively constraining the model SST. At 100 m depth, the temperature bias relative to the CARS climatology is smaller and of the opposite sign compared to the surface for both the 1/9° simulation (+2.23%) and the 1/45° (+1.07%) simulation. The correlation between model and observations at this depth remains high and the modelled standard deviation also compares well with the climatological value (r≈0.95, NSTD≈0.8-0.9). The normalised root mean square error for the simulated temperature fields at the surface and at 100 m depth is therefore low (NRMSE≈0.35). The mixed-layer depth (MLD) has a negative bias (−14.31%) with respect to the IFREMER climatology in the 1/9° simulation, while the spatial variability of the mean shows a very good fit (r>0.95, NRMSE≈0.25). In the 1/45° simulation the MLD bias is slightly larger (~ −22%) and also with respect to the spatial variability the fit is slightly worse (r≈0.9, NRMSE≈0.45). Note that the gridded MLD climatology has a coarse resolution (2° x 2°), which may contribute to the weaker correlation with the MLD in the 1/45° simulation.

Chlorophyll-a shows quite a substantial positive bias in both simulations relative to MODIS (>30%) as well as SeaWIFS (>60%) satellite observations (Fig. 2a,b). This positive bias is reduced in the 1/45° simulation by a factor of 2 compared to the 1/9° simulation. Despite the mean bias, the model fit is quite good with respect to the spatial chlorophyll variability relative to both MODIS and SeaWIFS data (NRMSE≈0.35-0.45). Modelled PP in the 1/45° simulation exhibits a negative bias relative to PP estimates derived from ocean color (~ −37%). The spatial correlation of this modelled PP to the satellite estimate is high, and the standard deviation is only slightly underestimated in the simulation (r≈0.9, NSTD≈0.8), resulting in a good model fit (NRMSE≈0.45, Fig. 2a).

Nitrate in both simulations shows a substantial bias at the surface (~ +51-61%) and a much smaller bias at 100 m depth (~ +17%), which is also apparent in figure 2c-e. There is however a high spatial correlation of the modelled mean nitrate fields with climatological fields (r≈0.8-0.9) and the standard deviation in the simulations slightly overestimated compared to the climatology (NSTD≈1.2-1.5). In general the model fit with respect to nitrate is improved slightly in the 1/45° simulation (NRMSE≈0.75, Fig. 2a) compared to the 1/9° simulation (NRMSE≈0.8, Fig. 2b).

To evaluate how the simulated mean horizontal and vertical temperature and nitrate gradients compare, we computed along-shore averaged mean sections of these variables from both simulations as well as from the CARS climatology (Fig. 2c-e). Above 100 m depth, which corresponds to about 13°C, the location of the simulated isotherms compares well with the climatology, but the model isotherms are slightly steeper within 200 km from the coast and less steep further offshore. Below 100 m depth, the vertical temperature gradient in the simulations is about 0.5°C m^{-1} higher than in the climatology.

The vertical nitrate gradient below 100 m depth is weaker in the simulations compared to the CARS climatology (Fig. 2c-e). The horizontal nitrate gradient reverses at ~ 150 m depth, a feature which is present in the modelled and the climatological nitrate fields. Despite the aforementioned bias of the simulated mean nitrate distribution, the horizontal and vertical nitrate gradients above 100 m depth compare well with the CARS climatology (Fig. 2c-e). We can therefore assume that the model can realistically represent the nitrate fluxes associated with upwelling and subduction, which
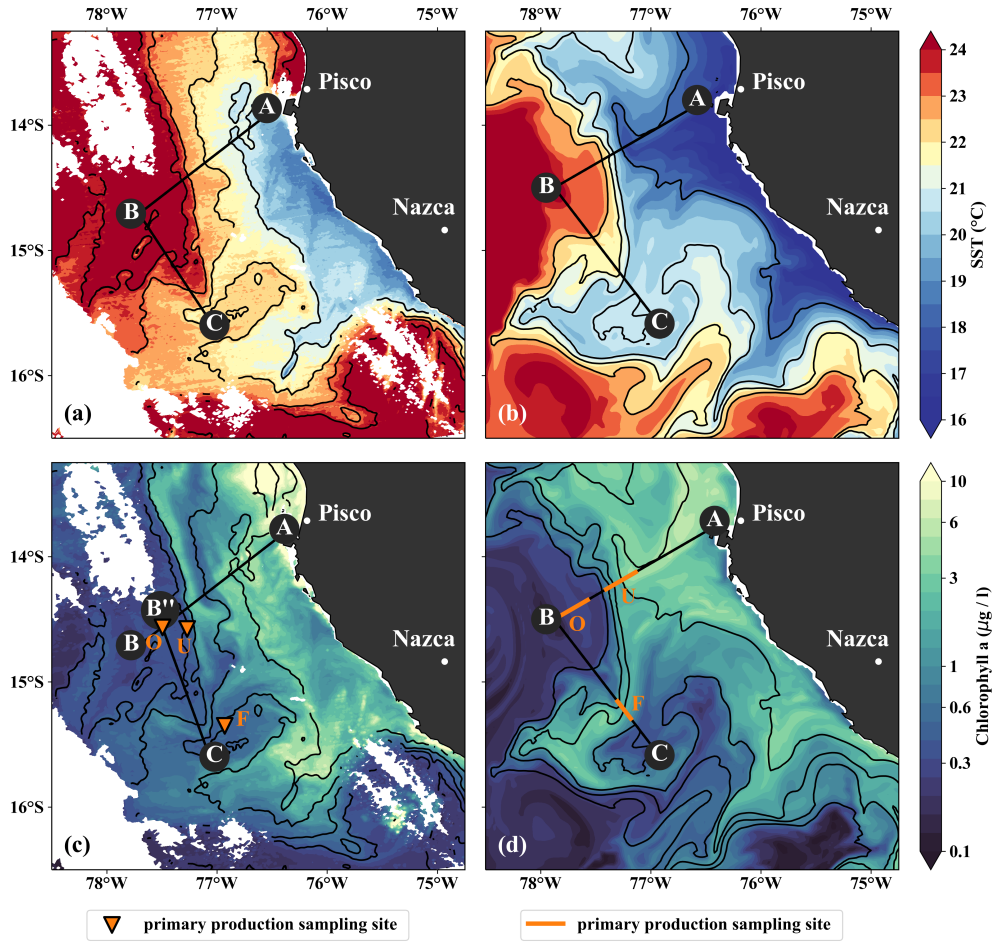
Figure 3. (a,b) Sea-surface temperature and (c,d) Surface chlorophyll in (a,c) observations on April 14, 2017 and in (b,d) the model simulation on April 5, 2017. Locations of vertical sections are superimposed (see Figs. 4; 5). Orange triangles in (c) indicate three sampling locations offshore (O), at the upwelling front (U) and in the filament (F) where primary production was measured. Orange lines in (d) indicate the corresponding locations used for comparison in the simulation. **The simulated fields represent 1-day averaged model output, which was chosen for the the horizontal gradients to be as sharp as possible and directly comparable to observations.**

occur predominantly in this depth range. For a more detailed evaluation of the 1/9° simulation please refer to Echevin et al. (2008), where a similar model configuration was used. The same simulations as in this study were used in a Master thesis by Hauschildt (2017), where an in depth model evaluation can be found.

3.2 Physical and biogeochemical upwelling structure in observations and simulations

The filament survey (Sec. 2.1) was carried out during the transition from Austral summer to fall on April 12 - 17, 2017. Being typical for the season, moderate southeasterly along-shore winds between 5 - 6 m s^{-1} near the coast and 11 - 14 m s^{-1} offshore were observed throughout the survey, which represents upwelling-favourable conditions (not shown). The most intense upwelling is often found in distinct cells near headlands and capes, indicated by along-shore minima of sea-surface temperature (SST). A well-known upwelling cell off Peru can be identified near 15 °S by its relatively low SST (18 °C) in a satellite image taken on April 14, 2017, 18:25 UTC (Fig. 3a). A strong cross-shore SST gradient exists between this coastal minimum and the warm offshore waters (24.5 °C). The maximum SST gradient (0.15 °C / km) is found 110 - 130 km offshore along the 23 °C isotherm and marks the location of the upwelling front. The offshore increase in SST is accompanied by an increase in salinity from 35.3 to 36.25 g kg^{-1} and an increase in mixed-layer depth from 5 m to 30 m, approximately following the $\sigma_\theta = 25$ kg m^{-3} isopycnal (Fig. 4a). Offshore of the upwelling front, a sharp thermocline with vertical temperature gradients of up to 0.4 °C m^{-1} across the base of the mixed layer is found (Fig. 4a). The deepest isopycnal that outcrops at the coast ($\sigma_\theta = 25.5$ kg m^{-3}) descends to 50 m depth 75 - 100 km offshore. The predominant water mass along the density surfaces that supply the coastal upwelling is the Equatorial Subsurface Water (ESSW, e.g. Silva et al., 2009) at a density of about $\sigma_\theta = 26.0$ kg m^{-3} and a salinity of 35.2 g kg^{-1} (Fig. 4b), which is transported poleward along the shelf by the Peru-Chile Undercurrent (PCUC; Gunther, 1936; Fonseca, 1989; Montes et al., 2010). The maximum poleward velocities of ~ 0.5 m s^{-1} are observed within 50 km from the coast at 20 - 100 m depth (Fig. 4c).

The observed physical variability in the upwelling region gives rise to biogeochemical variability on similar scales (Figs. 3c; 4d,e). Surface chlorophyll concentrations are enhanced inshore of the upwelling front (~ 5 mg m^{-3}) compared to offshore (~ 0.3 mg m^{-3}) due to nutrient-rich subsurface waters (15 - 20 μmol l^{-1} NO$_3$) that are brought to the surface in the coastal upwelling (Figs. 3c; 4d,e). Surface NO$_3$ concentrations decrease continuously by about 0.1 μmol l^{-1} per kilometer cross-shore distance to 5 μmol l^{-1} inshore of the upwelling front (Fig. 4e). Note that a local chlorophyll maximum occurs on the cold side of the upwelling front (~ 10 mg m^{-3}, Figs. 3c; 4d). Offshore of the upwelling front surface nutrients are depleted (< 1 μmol l^{-1} NO$_3$) and a strong vertical gradient of up to 2 μmol l^{-1} NO$_3$ m^{-1} is present across the base of the mixed-layer (Fig. 4e). As a result, the maxima in chlorophyll (7 - 10 mg m^{-3}, Fig. 4d, Table 1) and PP (~ 9 μmol C l^{-1} d^{-1}, Table 1) occur below the mixed-layer where nutrients are abundant (20 μmol l^{-1} NO$_3$, Fig. 4e). Below 80 m depth chlorophyll concentrations are low (< 0.2 mg m^{-3}) everywhere in the study area (Fig. 4d). Due to similarly low subsurface chlorophyll concentrations in the source waters on the shelf, surface chlorophyll concentrations remain relatively low (~ 1 mg m^{-3}) within 20 - 30 km from the upwelling center and only peak (4 - 6 mg m^{-3}) beyond this area (Figs. 3c; 4d). This illustrates that despite the clear inverse relationship of chlorophyll and SST on larger scales, small-scale chlorophyll variability is more complex and not consistently related with SST.

The characteristic structure of coastal upwelling in the physical fields is well reproduced in our simulations, but some differences exist (Figs. 4a-c,f-h). The location of the upwelling front 100 km offshore and the corresponding Δ SST maximum of 0.2 °C km^{-1} agrees well with both satellite images and in-situ measurements (Figs. 3a,b; 4a,f). The temperature and salinity
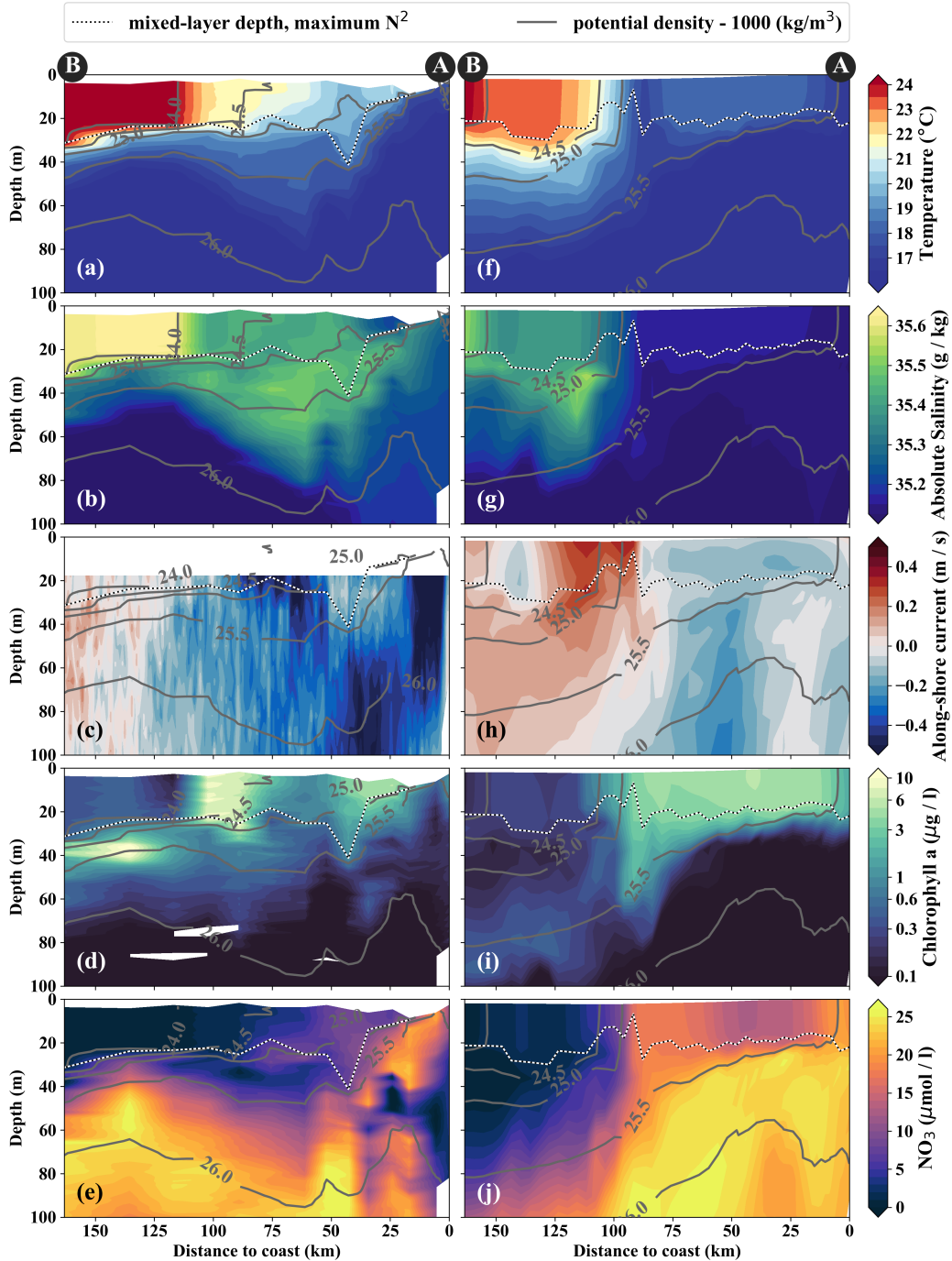
Figure 4. Cross-shore sections of (a,f) temperature, (b,g) salinity, (c,h) along-shore current, (d,i) chlorophyll and (e,j) nitrate in observations (a-e) and model simulation (f-j). Potential density contours are shown in grey and mixed layer depth is represented by the broken white/black line. Letters A and B indicate the section endpoints marked in Fig. 3. **The model sections represent 1-day averaged output on April 14, 2017, which was chosen for the horizontal and vertical gradients to be as sharp as possible and directly comparable to observations.**

distributions are similar overall to observations in the simulation, apart from a cold / fresh bias of the surface waters inshore of the upwelling front (Figs. 4a,b,f,g). Due to this bias the $\sigma_\theta = 25$ kg m^{-3} isopycnal outcrops 100 km offshore in the simulation and near the coast in the observations. The average mixed-layer depth in the simulation is ~ 20 m, very close to observed values offshore of ~ 100 km. However, the observed mixed-layer depth decreases to only ~ 5 m in the coastal upwelling patch, whereas such a shallow mixed-layer is not seen in the simulation (Fig. 4a,f). The southward velocities of ~ 0.3 m s^{-1} inshore of the upwelling front in the simulation that are associated with the surfacing undercurrent are similar to observations (Fig. 4c,h). However, the strongest southward flow (~ 0.3 m s^{-1}) in the simulation is weaker than observed (~ 0.5 m s^{-1}) and not located at the shelf but 55 km offshore. This is likely related to differences in the mesoscale variability, since an anticyclone is present immediately offshore of the upwelling patch in the simulation compared to a cyclonic eddy at approximately the same position in the observations (not shown). However, averaging over the period 2015 - 2016 yields an alongshore velocity of 13 cm s^{-1} in the core of the PCUC, which is close to the observed velocity (~ 14 cm s^{-1}, Chaigneau et al., 2013).

In the simulation, the upwelling structure also dominates the variability of the biogeochemical fields (Figs. 3d; 4i,j). Chlorophyll concentrations larger than 0.2 mg m^{-3} are found down to 80 m (100 m) in the observations (simulation), showing overall good agreement (Fig. 4d,i). Maximum surface chlorophyll in the observations (> 10 mg m^{-3}) and in the simulation (~ 8 mg m^{-3}) also match reasonably well. However, the cross-shore and vertical gradients of surface chlorophyll reveal notable differences between the observations and the simulation: local maxima of up to 10 mg m^{-3} are present along the nutricline and at the upwelling front located more than 100 km offshore in the observations, while chlorophyll concentrations in the simulation show no such maxima, are inversely related with SST and decrease almost continuously offshore and with depth (Fig. 3; 4d,i). Lastly, it is a common feature in satellite images of chlorophyll that concentrations remain relatively low (< 1 mg m^{-3}) in recently upwelled waters near the coast (30 km) and only increase to > 3 mg m^{-3} further offshore (Fig. 3c). This behaviour is to some degree reproduced in the simulation, but only within a much narrower (~ 10 km) region along the coast (Fig. 3d). The observed nutricline - here defined as the 10 μmol l^{-1} nitrate contour - is located between 20 m - 50 m depth in the open ocean and intersects the surface near the coast where upwelling occurs (Fig. 4e). The modeled nutricline is locally 100 m deep in the open ocean and also reaches the surface near the coast (Fig. 4j). Surface nitrate maxima of 5 μmol l^{-1} associated with filaments in the simulation are comparable to the observations.

In brief, the near-surface cross-shore gradients of temperature, nitrate and chlorophyll are well represented in the simulations. In the following section we will see how both observed and modelled cold filaments give rise to along-shore variability by advection across these gradients.

3.3 Physical and biogeochemical characterization of observed and modeled filaments

In the observations, cold filaments dominate the along-shore variability of physical and biogeochemical parameters near the surface (Figs. 3a,c; 5a-e). Two cold filaments with temperatures of 21.5 °C and 20.5 °C in their respective centers extend offshore from the upwelling center, separated by a ~ 30 km wide intrusion of 1 °C warmer water between them (Fig. 3a). **Their along-shore position matches with two SST minima (19 °C) at the coast, suggesting that they carry recently upwelled**
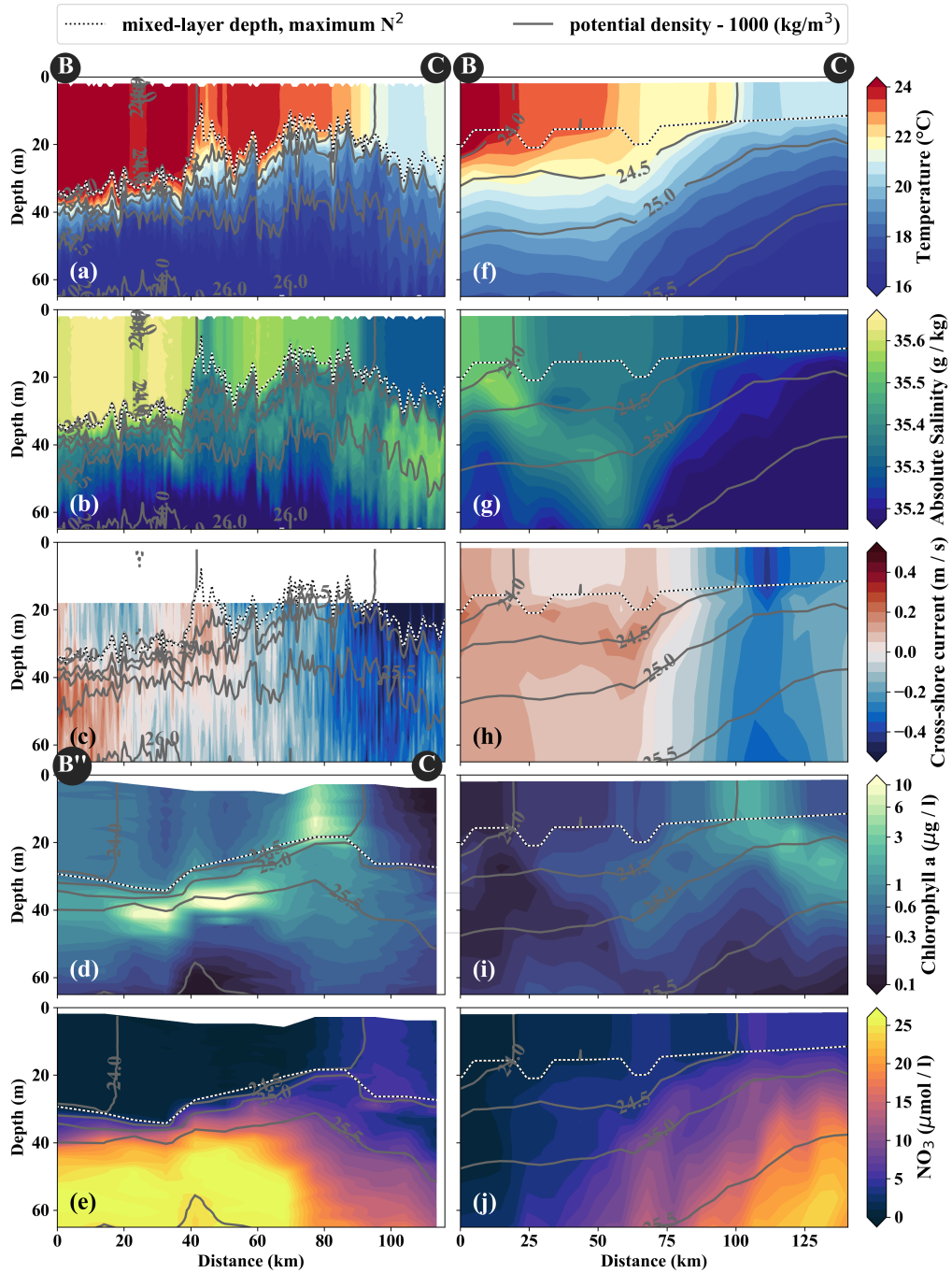
Figure 5. Same variables as in Fig. 4. Note the slightly different endpoints of the physical and biogeochemical section in the observations (see B and B" in Fig. 3). **The model sections represent 1-day averaged model output on April 14, 2017, which was chosen for the the horizontal and vertical gradients to be as sharp as possible and directly comparable to observations.**

17

water. In the following we focus on the relatively narrow (10 - 20 km) northern filament at 15.25 °S, 77 °W because of multiple available physical and biogeochemical measurements. The filament can be identified in satellite SST images already on March 22 and changed its position only by $\mathcal{O}(10)$ km until it was sampled on April 15 (not shown). The associated SST fronts are present the entire time, but vary in strength. The physical structure of the filament and the distribution of the biogeochemical parameters **are** characterized in the following.

The cold filament is associated with along-shore variability of the physical and biogeochemical fields in the mixed layer (Fig. 5a-e). It is characterized by a pronounced minimum in temperature (20 °C) and salinity (35.2 $g\,kg^{-1}$) in the mixed-layer at the southern end (110 km) of transect PHY (Fig. 5a,c). The minimum temperature found in the filament on transect PHY is at least 1.5 °C colder than suggested by the satellite SST (Figs. 3a, 5a). This mismatch is likely related to the diurnal cycle of solar insolation and differential heating, as PHY crossed the filament in the early morning but the SST image was recorded the day before shortly after noon. The low salinity is characteristic of ESSW along the shelf (see Sec. 3.2) and thus indicates that the filament contains recently upwelled water which is transported to the open ocean by an offshore flow of up to 0.5 $m\,s^{-1}$ within the mixed-layer (Figs. 5c). The subsurface flow is mainly offshore at the southern end of transect PHY as opposed to onshore flow at its northern end, which is related to a cyclonic mesoscale eddy (not shown). Weak stratification below the filament between the 24.5 $kg\,m^{-3}$ and 25 $kg\,m^{-3}$ isopycnals (not shown) points to water that has been in the mixed-layer recently and could indicate subduction by submesoscale frontal processes. Low salinity anomalies (35.3 $g\,kg^{-1}$) in the same density range below the filament support this hypothesis (Fig. 5b).

Along with the physical properties, the filament creates along-shore variability of the biogeochemical parameters (nitrate, chlorophyll) by advecting recently upwelled water into the open ocean (Figs. 5d,e). Nutrient concentrations in the mixed-layer are enhanced in the filament (4 - 7 $\mu mol\,l^{-1}$ NO_3) compared to the surrounding waters (< 1 $\mu mol\,l^{-1}$ NO_3) while the highest nitrate concentrations are found near the filament's northern edge (Fig. 5e). **A local NO_3 maximum is located at the base of the mixed-layer (Fig. 5e).** Despite available nutrients chlorophyll concentrations are very low (< 0.1 $mg\,m^{-3}$) within the filament, comparable to those found below the photic zone (Fig. 5d). PP in the filament is still relatively high with a maximum (7.5 $\mu mol\,C\,l^{-1}\,d^{-1}$) at 10 m depth within a 35 m deep mixed-layer (Table 1). High chlorophyll concentrations (~ 8 $mg\,m^{-3}$) are only found at the northern edge of the filament 75 km along transect BIO (Fig. 5d). Outside the filament, surface waters are nutrient-depleted (< 0.2 $\mu mol\,l^{-1}$) while just below the mixed-layer high nutrient concentrations (25 $\mu mol\,l^{-1}$ NO_3) are present (Fig. 4e). The maxima in chlorophyll (> 10 $mg\,m^{-3}$) and PP (9.4 $\mu mol\,C\,l^{-1}\,d^{-1}$) are therefore located below the mixed-layer (~ 40 m) where nutrients are abundant (Fig. 5d,e; Table 1). Below 80 m depth, chlorophyll concentrations are low everywhere along the transect (< 0.1 $mg\,m^{-3}$) and primary production is low (< 0.1 $\mu mol\,C\,l^{-1}\,d^{-1}$) at the upwelling front, offshore and in the filament (Figs. 3c, 4d; Table 1). Notably, surface PP in the filament is a factor 2 higher than at the upwelling front (3.6 $\mu mol\,C\,l^{-1}\,d^{-1}$), while the latter dominates the offshore chlorophyll variability in satellite images with surface chlorophyll concentrations of about a factor 4 higher than in the filament (Fig. 3c).

The position and shape of simulated filaments is determined largely by the mesoscale eddy field, which evolves freely in the simulation and can therefore not be expected to correspond to the variability in the real ocean at any given time. The occurrence of major upwelling events and their effect on the variability of fronts and filaments, however, is closely

related to the wind forcing of the model, which was derived from satellite-based, daily ASCAT scatterometer winds. We therefore picked simulated filaments that were as close as possible in space and time to the observations, which were then taken to be representative of the area and season when the observations were carried out. The chosen filaments are comparable in scale to the observed cold filament, which had an offshore extent of 150 km - 200 km (Fig. 3a,b). Similar to satellite images, the simulated surface fields of SST and chlorophyll show two separate filament structures originating in the upwelling patches off Pisco and Nazca on April 5, 2017 (Fig. 3b,d). Of the two separate filament structures that are present, for comparability we focus here on the northern filament whose location near the upwelling front is similar to the one observed. The modelled filament is associated with pronounced along-shore variability in the physical and biogeochemical fields (Fig. 5, f-j). Offshore velocities are present in the filament down to 100 m depth, with a maximum located in the mixed-layer (0.4 m s^{-1}, Fig. 5h). Surface minima of temperature (20 °C) and salinity (35.25 g kg^{-1}) and maxima of chlorophyll and nitrate are associated with the filament (Fig. 5f-j). Enhanced nitrate concentrations of 5 μmol l^{-1} are present in the filament and a shallowing of the nutricline is found in the same location, associated with doming isopycnals between $\sigma_\theta = 25$ kg m^{-3} and $\sigma_\theta = 25.5$ kg m^{-3} (Fig. 5j). Elevated chlorophyll concentrations of 2 mg m^{-3} are found at its northern edge, marked by the $\sigma_\theta = 24.5$ kg m^{-3} isopycnal outcrop (Fig. 5i). **PP in the modelled filament is enhanced relative to the surrounding offshore waters, similarly to observations (Table 1).** However, the modelled PP is only enhanced where high chlorophyll concentrations are found, which is not the case for the observations where high PP inside the filament coincides with low chlorophyll. Vertical gradients of PP are also different in the model compared with observations: While there is a strong chlorophyll maximum below the mixed-layer that is associated with higher PP than at the surface, subsurface maxima of chlorophyll are rare and weak in the simulation and PP generally decreases with depth. Despite these differences, the modelled mixed-layer PP has a realistic order of magnitude offshore, at the upwelling front and in the filament (Table 1).

In summary, the simulation exhibits upwelling filaments that are similar in lateral and horizontal scale and offshore extent to those observed. Our direct rate measurements indicate that PP in the modelled filaments is comparable to observations. Despite very low chlorophyll concentrations (< 0.1 mg m^{-3}) in the observed filament, surface PP is by a factor 2 higher than at the upwelling front. This highlights the necessity of measuring PP in addition to chlorophyll for model validation to ensure a realistic representation of the underlying processes.

3.4 Timescales of nutrient transport and uptake in observations and models

The model is able to reproduce realistic mixed-layer nitrate concentrations as well as mixed-layer PP rates offshore in the filaments, suggesting that the simulated rate of nitrate uptake (i.e. new production) is realistic as well (Figs. 4e,j; 5e,j; Table 1). However, it must be noted that our PP in situ estimates do not discriminate between new PP and regenerated PP resulting from ammonium uptake (see discussion section). Assuming that the simulated nitrate uptake rate is realistic, we can use the model to analyze the physical and biogeochemical processes in the upwelling system in more detail and over a larger area. To do this, we released virtual floats in our submesoscale-permitting simulation. By tracking biogeochemical variables along float trajectories, we studied the biological response to upwelling and subduction in a

Table 1. Observed and modelled primary production for different dynamical regimes, each at 3 different depths. The first sample was always taken at 10 m, while the remaining two were placed in the chlorophyll maximum below the mixed-layer (25 m - 40 m, ~ 10% surface PAR) and a chlorophyll minimum below the photic zone (70 m - 80 m, ~ 1% surface PAR). Sampling sites and the corresponding model locations used for comparison are marked with letters O, U and F in Fig. 3c,d. Standard deviation represents triplicate samples for the PP observations, ± 3 m bottle depth for the corresponding chlorophyll fluorescence profiles and differences between individual grid points for the model data.

Regime	Observations			Model		
	Depth (m)	Chlorophyll ($\mathrm{mg\,m^{-3}}$)	Primary production ($\mu\mathrm{mol\,C\,l^{-1}\,d^{-1}}$)	Depth (m)	Chlorophyll ($\mathrm{mg\,m^{-3}}$)	Primary production ($\mu\mathrm{mol\,C\,l^{-1}\,d^{-1}}$)
Offshore	10	0.45 ± 0.10	2.12 ± 0.044	10	0.24 ± 0.038	1.01 ± 0.134
	35	7.64 ± 3.922	9.43 ± 1.402	(10% PAR) 40	0.15 ± 0.009	0.19 ± 0.033
	70	0.11 ± 0.012	0.09 ± 0.031	(1% PAR) 82	0.39 ± 0.029	0.08 ± 0.005
Upwelling Front	10	3.49 ± 0.302	3.59 ± 0.721	10	2.80 ± 1.348	5.74 ± 1.925
	40	7.42 ± 1.299	5.84 ± 0.757	(10% PAR) 18	2.52 ± 1.528	1.99 ± 1.016
	80	0.13 ± 0.025	0.08 ± 0.005	(1% PAR) 35	1.90 ± 1.307	0.30 ± 0.192
Filament	10	0.66 ± 0.051	7.50 ± 1.418	10	1.43 ± 0.322	3.78 ± 0.672
	25	0.10 ± 0.016	0.25 ± 0.021	(10% PAR) 22	1.07 ± 0.353	1.14 ± 0.434
	80	0.00 ± 0.002	0.03 ± 0.001	(1% PAR) 47	0.22 ± 0.014	0.04 ± 0.002

reference frame following the upwelled water. The upwelled floats originate at depths between 20 - 120 m, the maximum depth agreeing well with the maximum depth of outcropping isopycnals (Figs. 4; 6a). Using the physical and biogeochemical properties averaged over all floats after grouping into subducted and not subducted ones, we can diagnose the biological response to upwelling and the corresponding timescale (Fig. 6a-e). **Phytoplankton growth in PISCES increases exponentially with**

5 **photosynthetically active radiation (PAR) and also increases as a function of temperature (subsection 2.5, equation 5).** PP and chlorophyll along the float trajectories thus increase exponentially a few days before upwelling as the floats move to shallower depths where both PAR and temperature are higher and phytoplankton biomass accumulates (Fig. 6a-c). For the floats that are not subducted and remain within the photic zone chlorophyll peaks 15.3 days after upwelling ($4.1\ \mathrm{mg\,m^{-3}}$), followed by a peak in PP after 17.1 days ($13.1\ \mu\mathrm{mol\,C\,l^{-1}\,d^{-1}}$). For the subducted floats these timescales are slightly shorter,

10 chlorophyll peaks after 14.5 days ($2.0\ \mathrm{mg\,m^{-3}}$) and PP peaks after 13.4 days ($4.0\ \mu\mathrm{mol\,C\,l^{-1}\,d^{-1}}$).

 The fate of upwelled floats is closely related to their change in temperature after upwelling, thus the correct representation of the temperature gradient in the model is crucial (Fig. 3a,b). Water that is warmed rapidly by surface heat fluxes or mixed with warmer offshore waters remains at shallower depths where sufficient light allows for PP and nutrient uptake. In contrast, floats with little temperature change after upwelling are more quickly removed from the photic zone by subduction.

Average PP of the subducted floats reduces to 0.1 μmol C l^{-1} d^{-1} after 20 days, because they are all located below the photic zone at this time by design of our diagnostics (Fig. 6b). In contrast, average PP of the floats that are not subducted is still at 6.4 μmol C l^{-1} d^{-1} after 20 days. Nitrate concentrations of subducted floats reduce to 16.5 μmol l^{-1} which is 1.5 μmol l^{-1} lower than upwelled concentrations (Fig. 6e). These numbers show that along the subducted trajectories only a small fraction

5   of the upwelled nitrate is taken up by phytoplankton. In contrast, along the trajectories of those floats that remain in the photic zone phytoplankton can utilise more nitrate indicated by nitrate concentrations of 12.0 μmol l^{-1} 20 days after upwelling, which is 7.1 μmol l^{-1} lower than upwelled concentrations. **Using the subduction ratio (Equation 7) defined in subsection 2.5, we estimate that 20 days after being upwelled 40.6% of the upwelled nitrate is subducted (Fig. 6f). More detailed statistics of the float experiment are given in Table 2.**

10   Nitrate concentrations in the observed filament around 150 km offshore are only 20 - 50% of those measured near the coast and decrease continuously with offshore distance on cross-shore transect CROSS (Fig. 3e). This suggests that upwelled nitrate fuels a substantial amount of the observed PP. To estimate a timescale over which the observed nitrate uptake occurs, we use offshore velocities of 0.3 - 0.5 m s^{-1} observed in the filament which leads to an advection time of 3.5 - 5.8 days from the upwelling center to reach the filament 150 km offshore (this timescale represents a lower bound since the actual path that

15   the water parcel took is unknown and likely longer than a straight line). Initial nitrate concentrations of 15 μmol l^{-1} in the upwelled water and 5 μmol l^{-1} in the filament yield a nitrate reduction of 10 μmol l^{-1} over this time period, which is well within the uncertainty of the modelled estimate.

3.5   Effect of resolution on the biogeochemistry of the Peruvian upwelling

20   With the purpose of quantifying the impact of the different dynamics at submesoscale-permitting (1/45°) resolution on upwelling and subduction of nutrients, we repeated the above float experiment using the mesoscale (1/9°) model flow field and compared both results (Table 2). In the mesoscale experiment, the mean nitrate concentration of upwelled floats is **2.4 μmol l^{-1}** higher than in the submesoscale experiment. For the subducted floats, this higher initial nitrate concentration is overcompensated by a higher uptake along the float trajectories so that offshore nitrate concentrations are 2 μmol l^{-1} lower in the mesoscale

25   simulation. For the floats that were not subducted, increased nitrate uptake in the mesoscale simulation also overcompensates the initially higher concentrations, so that offshore nitrate concentrations are 5 μmol l^{-1} lower in the 1/9° compared to the 1/45° simulation. This higher nitrate uptake for both subducted and not subducted floats in the 1/45° simulation can be explained by on average deeper float trajectories (Fig. 7) and therefore lower light levels and lower PP compared to the 1/9° simulation. Accordingly, subduction of upwelled nitrate is increased by 13.9 % in the 1/45° simulation compared to the 1/9°

30   simulation, while the maxima of PP and chlorophyll along the averaged trajectories are reduced by 5.3 μmol C l^{-1} d^{-1} and 2.2 mg m^{-3}, respectively (Table 2).

This increased subduction in the 1/45° simulation is also apparent in the vertical float distribution 20 days after upwelling (Fig. 7). The vertical maximum of the float distribution is located in the top 5 m for the both simulations, but below this surface peak the distributions are very different: In the 1/45° simulation the majority of floats is evenly distributed between 5 - 50 m
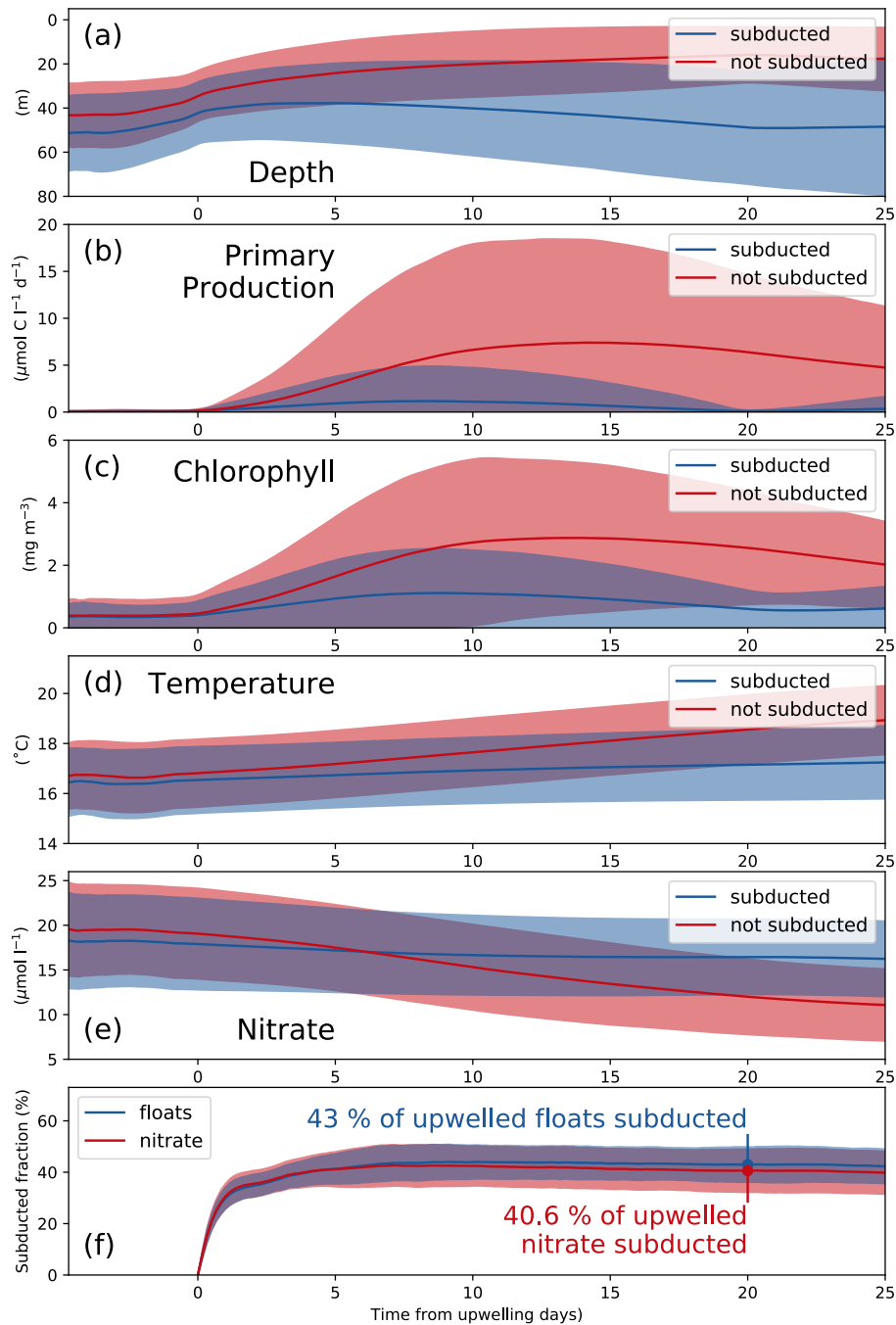
Figure 6. (a) Depth, (b) primary production, (c) chlorophyll, (d) temperature and (e) nitrate averaged over all subducted (solid) and not subducted (dashed) floats from 20 ensemble members. Blue and red shading indicates the range of ± 1 standard deviation based on all subducted and not subducted floats, respectively. (f) Subducted fraction of floats and nitrate. Shaded areas represent the range of ± 1 standard deviation based on 20 ensemble members.

22

Table 2. Diagnosed variables from the virtual float ensembles in the 1/45 ° and 1/9 ° simulations. "Peak" values represent the maximum of the average over floats of one simulation.

Parameter		1/45 °	1/9 °	mean difference
Upwelled floats (absolute)		5048.9 ± 1108.0	3619.7 ± 964.1	-1429.3
Subducted floats (absolute)		2158.0 ± 559.8	1149.9 ± 349.3	-1008.1
(relative)		$43.0 \pm 6.9\,\%$	$32.0 \pm 5.7\,\%$	-10.9 %
Upwelled NO_3 concentration ($\mu mol\,l^{-1}$)		17.5 ± 1.4	19.8 ± 0.8	+2.4
Subducted NO_3 (relative)		$40.6 \pm 8.4\,\%$	$26.7 \pm 6.0\,\%$	-13.9 %
Floats out of domain (absolute)		48.9 ± 34.0	0	-48.9
(relative)		$1.0 \pm 0.8\,\%$	0	-1.0 %
Peak primary production	- subducted floats	4.0 ± 1.2	3.2 ± 1.0	-0.8
($\mu mol\,C\,l^{-1}\,d^{-1}$)	- not subducted floats	13.1 ± 2.5	19.7 ± 3.3	+6.6
	- all floats	9.1 ± 1.7	14.5 ± 3.0	+5.3
Peak chlorophyll	- subducted floats	2.0 ± 0.4	2.6 ± 0.7	+0.6
($mg\,m^{-3}$)	- not subducted floats	4.1 ± 0.6	6.6 ± 0.8	+2.6
	- all floats	3.1 ± 0.4	5.3 ± 0.7	+2.2
Time of peak primary production	- subducted floats	13.4 ± 1.4	13.3 ± 2.5	-0.1
(days after upwelling)	- not subducted floats	17.1 ± 0.9	16.1 ± 1.9	-1.0
	- all floats	15.4 ± 1.0	15.2 ± 1.8	-0.2
Time of peak chlorophyll	- subducted floats	14.5 ± 1.3	14.3 ± 3.1	-0.2
(days after upwelling)	- not subducted floats	15.3 ± 1.4	14.3 ± 2.0	-1.0
	- all floats	14.9 ± 1.1	14.3 ± 2.2	-0.6

depth, while in the 1/9 ° simulation the float abundance sharply decreases downward from a much more pronounced surface peak. The maximum depth reached by float trajectories is deeper by about 30 m in the 1/45 ° simulation (Fig. 7). **Comparing the same virtual float experiment in different simulations illustrates well the relative changes in subduction and their biogeochemical impacts, but this Lagrangian approach is restricted to short integrations during one season and is less suited to obtain estimates of absolute changes of the time-averaged model fields.**

The impact of increased horizontal resolution on the long-term averaged biogeochemical fields can be approximated based on the difference between the coarse- (1/9 °) and high-resolution (1/45 °) simulations. In a first-order assessment, this dif-ference can be taken to represent the influence of submesoscale frontal processes and the associated horizontal and vertical
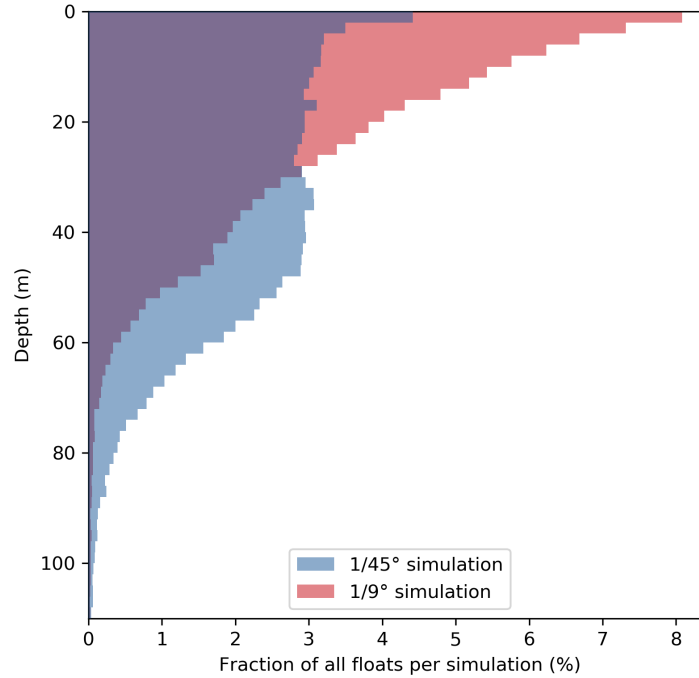
Figure 7. Vertical distribution of all upwelled floats from the float experiment ensemble 20 days after upwelling in the 1/9° and 1/45° simulations. Histograms were generated using 2 m vertical bins.

eddy-fluxes that are additionally resolved in the high-resolution simulations, an assumption that is justified by the pronounced increase in eddy kinetic energy by a factor of 2 from coarse to high resolution (Fig. 8a). The changes in nitrate due the effect of submesoscale-permitting resolution in the simulations are greatest within 25 km from the coast in the upper 200 m of the water column, where a pronounced decrease in nitrate (-2.5 $\mu\mathrm{mol\,l}^{-1}$, Fig. 8b) is apparent. These reduced subsurface nitrate concen-

5   trations in the 1/45 ° compared to the 1/9 ° simulation are consistent with ~ 2 $\mu\mathrm{mol\,l}^{-1}$ lower nitrate concentrations of upwelled floats (Table 2). **In a tongue that extends from this minimum ~ 250 km offshore along the nutricline, a smaller decrease in nitrate (~ -1.5 $\mu\mathrm{mol\,l}^{-1}$, Fig. 8b) is seen. Offshore of this negative change, an increase in nitrate (~ 1.5 $\mu\mathrm{mol\,l}^{-1}$) is apparent around 100 m depth. The positive change in nitrate offshore together with increased eddy kinetic energy (EKE) in the 1/45 ° simulation suggests that an increase in the cross-shore nitrate flux takes over once the nitrate is**

10   **removed from the surface (Fig. 8a,b). The horizontal patterns of nitrate change are largest in regions of increased eddy kinetic energy (not shown). At a depth of 300 m to 500 m nitrate increases near the coast (~ 2 $\mu\mathrm{mol\,l}^{-1}$), directly below the strong nitrate decrease in the top 200 m (~ -2.75 $\mu\mathrm{mol\,l}^{-1}$). A plausible explanation for this pattern is that due to increased offshore transport in the submesoscale simulation sinking organic matter sediments on deeper shelf areas,**

24

out of reach of the upwelling source waters. This would result in a downward redistribution of nitrate similar to the "nutrient leakage" described in Gruber et al. (2011). However, small differences in the alongshore mean circulation along the continental slope (not shown) may also modify the nitrate content of the water masses. Disentangling these processes is beyond the scope of the present work. A decrease in chlorophyll of 1 mg m^{-3} near the coast and 0.3 mg m^{-3} 300 km offshore between the 1/45° and 1/9° simulations is seen at the surface (Fig. 8d). This decrease in surface chlorophyll coincides with an increase in surface nitrate ($+0.5$ μmol l^{-1}), pointing to reduced nitrate uptake due to limitation of phytoplankton growth by nutrients other than nitrogen. In order to understand the reason for this model behaviour, we diagnosed which nutrient is limiting primary production in the simulation for the surface layer at every grid point and time step. We have identified a decrease of surface iron concentrations by 50% in the 1/45° simulation (Fig. 8c), leading to a shift from nitrogen to predominantly iron limitation in a 50 km wide band close to the coast over most of the year (not shown). Given that the coastal area is where most production occurs, increased subduction of upwelled iron in addition to nitrate subduction in the 1/45° simulation could contribute to the reduced productivity at the surface.

4   Discussion

Using an integrated approach of in situ observations and modelling, we estimated that 40.6 % of the upwelled nitrate is subducted without being utilised by phytoplankton. **While the agreement between observed and modelled synoptic variability introduced by filaments and fronts lends some confidence to our results, there are uncertainties and limitations which will be discussed in the following.**

We use the fraction of all upwelled floats that **have been subducted 20 days after upwelling** for quantifying changes in the associated nutrient fluxes. These float trajectories represent only advective fluxes while diffusion and surface-mixing are not resolved, yet at submesoscale-permitting resolution and for short integration times it is reasonable to assume that the advective fluxes are dominant and our approach is justified. **A mean bias of the physical and biogeochemical fields in the 1/45° simulation (see section 3.1) could have an effect on the results of our Lagrangian analysis. The 17°C isotherm is steeper near the coast in the 1/45° simulation compared to the CARS climatology (Fig. 2c,e), resulting in a negative SST bias of ∼ −3% (Fig. 2a, Fig. 3a,b) that is common in ROMS simulations (e.g. Echevin et al., 2008). More importantly for our study, we identified a positive nitrate bias of ∼ 61% at the surface and ∼ 17% at 100 m depth relative to the CARS climatology (Fig. 2a). A positive nitrate bias of similar magnitude (6 - 8 μmol l^{-1}) has also been documented by Espinoza-Morriberon et al. (2017) in their regional PISCES simulations off Peru. The much higher surface bias compared to 100 m depth can be explained by the steeper isotherms near the coast where the nitrate bias is largest, since the nitracline approximately coincides with the thermocline (Fig. 2c,e). The positive nitrate bias suggest an overestimation of the upwelling nitrate fluxes. Since the nitrate concentrations in the coastal upwelling are generally high and thus not limiting PP, it is likely that the nitrate bias does not have a substantial effect on the uptake of nitrate due to PP before subduction. PP in the simulation was also compared to synoptic in-situ measurements (Table 1) and mean satellite estimates (Fig. 2a), and the simulated filaments still contain ∼ 5 μmol l^{-1} nitrate offshore which is**

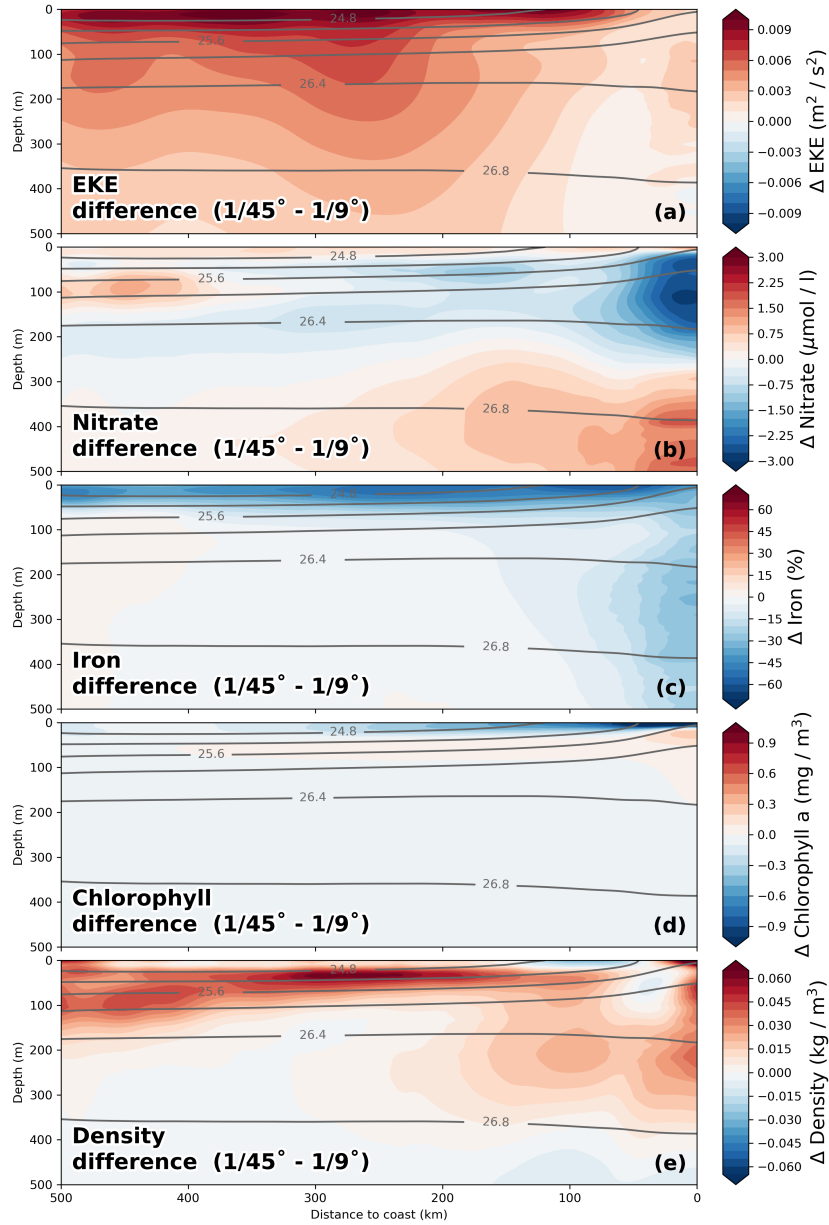**Figure 8.** Relative changes in (a) Nitrate (b) Iron (c) Chlorophyll (d) Temperature and (e) eddy kinetic energy (EKE) between the 1/9° and 1/45° simulations calculated as $\Delta X = X_{1/45} - X_{1/9}$. EKE was calculated relative to a 6 month running mean. All fields were averaged on depth levels in along-shore direction with 25 km cross-shore bins in a coastal band of 500 km width between 10.5 °S and 17.5 °S over the period 2015 - 2016. Grey lines represent potential density averaged over the 1/9° and 1/45° simulations.

confirmed in our observations. This further increases our confidence that the nitrate uptake in the simulation is realistic but occurs within a positively biased absolute value range.

The nitrate bias, however, can still impact our estimate of the subducted nitrate fraction (Equation 7, Fig. 6f). To obtain a first-order estimate of the uncertainty due to this bias, we compute the subduction ratio again from averaged mean

5 quantities along the float trajectories. In this case equation (7) can be simplified to

$$
\text{ratio} = \frac{F_{\text{subducted}}}{F_{\text{upwelled}}} \left(1 - \frac{\langle \Delta \text{NO}_3 \rangle_{\text{subducted}}}{\langle \text{NO}_{3,t_0} + B_{\text{NO}_3} \rangle_{\text{subducted}}} \right)
\tag{8}
$$

where F is the respective number of upwelled and subducted floats and angled brackets denote averages over all

10 subducted float trajectories. The subducted float fraction $F_{\text{subducted}}/F_{\text{upwelled}}$ is 43% in our study and not affected by the nitrate bias. The second term in the parentheses reduces this subducted float fraction, which explains why the subducted nitrate fraction (red line in figure 6f) is always lower than the subducted float fraction (blue line in figure 6f). The reducing term represents the ratio between the nitrate uptake after upwelling ΔNO_3 and the sum of upwelled nitrate concentration NO_{3,t_0} and nitrate bias B_{NO_3}. Because the nitrate bias occurs in the denominator, it leads to an

15 overestimation of the subducted nitrate fraction. To approximate this error, we insert averaged values from our float experiments (Fig. 6e) into equation (8): For the ensemble mean values of our float experiment (ΔNO_3=1.5μmol l^{-1}, NO_{3,t_0}=16.5μmol l^{-1}) and no bias we obtain a subducted nitrate fraction of 39%, close to our original estimate (40.6%, Fig. 6f). Correcting for an assumed positive nitrate bias of 65% (ΔNO_3=1.5μmol l^{-1}, NO_{3,t_0}=10μmol l^{-1}) we obtain a subducted float fraction of 36.5%. This calculation still assumes that ΔNO_3 is unbiased, but in reality there may be a

20 negative bias due to the ∼ −37% negative bias of PP described above. Assuming that ΔNO_3 also exhibits a −37% negative bias and correcting for it (ΔNO_3=2.4μmol l^{-1}, NO_{3,t_0}=10μmol l^{-1}) yields a subducted nitrate fraction of 30.5%, which can be viewed as a lower limit of the uncertainty range.

In summary, we approximate that the mean biases of nitrate and PP in the 1/45° simulation likely result in an overestimation of the subducted nitrate fraction with a lower bound of 30.5% of upwelled nitrate being subducted. It should

25 also be noted that not all upwelled floats reach the surface at the time of upwelling but instead originate from depths within the photic zone were the nitrate bias is smaller, which may alleviate the error associated with this bias to some extent. Beyond this, it is possible that nitrate in the CARS climatology is biased low due to undersampling of high-nutrient conditions. Espinoza-Morriberon et al. (2017) suggest that their extensive in-situ nitrate and surface chlorophyll observations off Peru likely still suffer from insufficient sampling resolution.

30 The physical and biogeochemical observations of the upwelling center near 15°S off Peru agree well with previous studies. Nitrate concentrations of ∼ 20 μmol l^{-1} at the coast and 5 μmol l^{-1} offshore that were observed in this study are in good agreement with previous measurements in the upwelling near 15°S off Peru and further north on the Peruvian shelf that range between 0.89 - 17.1 μmol l^{-1} (Blasco et al., 1984; Dengler, 1985; Macisaac et al., 1985; Fernández et al., 2009; Kalvelage

et al., 2013). The observed cold filament described in this study exhibited high nitrate and low chlorophyll concentrations in its core but enhanced chlorophyll at the front separating it from the warm offshore waters (Fig. 5). The same pattern was observed by Hosegood et al. (2017) in a similar filament off Mauritania (150 km offshore extent, 0.4 m s^{-1} offshore velocity), suggesting that these may be general features of EBUS cold filaments.

5   The range of PP rates that were determined experimentally from incubations (Table 1) is very close to measurements by Dengler (1985) acquired during April-June 1976 in the upwelling center near 15°S (4 - 16 μmol C l^{-1} d^{-1}), increasing confidence in our results. In October 2005, Fernández et al. (2009) observed a similar range of PP rates in the top 25 m of the water column slightly north (3 - 16.5 μmol C l^{-1} d^{-1}; 11 - 12°S) and south (1 - 3.5 μmol C l^{-1} d^{-1}; 16 - 18°S) of our study area. The PP rates diagnosed in the biogeochemical model simulations are close to our observed PP rates and

10   represent well the horizontal variability between different dynamical regimes in the study region (Table 1), except for the offshore waters where the modelled subsurface PP is likely too low. Satellite-based estimates of mean NPP suggest that the vertically integrated PP in the model has a negative bias (~ −37%, Fig. 2a).

Besides, our observations of PP rates in the filament do not distinguish between regenerated production from ammonium and new production from nitrate (Dugdale and Goering, 1967). Fernández et al. (2009) show that regenerated

15   nitrogen can locally account for as much as 50% of surface primary production in southern Peru. However, nitrate concentrations measured in the filament 150 km offshore are only 20 - 50% of those measured near the coast and nitrate appears to decrease with offshore distance on transect CROSS (Fig. 4). This is an indicator that a substantial amount of PP in the region of the filament survey near 15°S is fuelled by newly upwelled nitrate. We estimated using observed velocities that a reduction in nitrate concentrations by 10 μmol l^{-1} occurs over the course of 3.5 - 5.8 days while the water

20   is advected offshore. Assuming this reduction in nitrate concentrations occurs only due to phytoplankton growth in a closed volume would require PP rates of 11.4 - 18.9 μmol C l^{-1} d^{-1} (using a C : N ratio of 6.625 after Redfield, 1963). This estimate is higher than the ~ 7.5 μmol C l^{-1} d^{-1} measured in the filament, possibly pointing to nitrate being removed from the surface waters due to subduction and diffusion processes. Admittedly, large uncertainties are associated with this crude estimate since it is likely that (1) PP in the upwelled water did not remain constant, (2) the ratio of C and N uptake does not correspond

25   exactly to the Redfield ratio, (3) the water parcel did not travel offshore in a straight line, (4) was subject to mixing with the surrounding water and (5) local remineralisation of nutrients took place. Nevertheless, it provides a useful illustration that advected nitrate from the upwelling patch near the coast is more than sufficient to support the observed phytoplankton growth inside the filament. It is therefore reasonable to assume that a substantial fraction of PP occurring within the filament is fuelled by newly upwelled nitrate.

30   Along-shore variability of PP in the simulation is closely related to chlorophyll concentrations, while the observed relationship of PP and chlorophyll is less clear (Table 1). Investigating the reasons for this discrepancy is beyond the scope of this study and left for future work, but we can speculate that it is related to the relatively simple parameterisation of primary production in PISCES (see section 2.5). For example, changes of the phytoplankton physiology or species composition of the phytoplankton community are not modelled, which would likely allow stronger variations

35   of the chlorophyll to carbon ratio of phytoplankton (section 2.5, equation 5). Another missing process is the aging or

health of the phytoplankton population, which could slow down PP while chlorophyll concentrations remain high and thereby decouple the two parameters. Note that a new version, PISCES-quota (Kwiatkowski et al., 2018) will be able to represent more elaborate phytoplankton stages in future studies. Vertically, the modelled PP strictly decreases with larger depth corresponding to lower light levels, while in the observations subsurface maxima of PP are found offshore and at the
5   upwelling front (Table 1). The subsurface chlorophyll maximum is too weak and diffuse in the simulations, which is consistent with this difference in the vertical distribution of PP. This could be partly related to dynamical bias in the simulations: Near-surface stratification at the base of the mixed-layer is by a factor of 2-3 lower in the model than in the observations, which likely results in a too diffuse offshore nutricline and contributes to the weak subsurface chlorophyll maximum. For the reasons mentioned above, subsurface PP in the offshore waters is likely too low in our simulations.

10   We estimated the impact of submesoscale frontal processes by comparing virtual float experiments in the 1/9° and 1/45° simulations and found that subduction of nitrate increases by 13.9 % at submesoscale-permitting resolution. A decrease in mean PP by about one-third going from 1/9° to 1/45° resolution is also seen along float trajectories (Table 2). The difference between two-year averaged fields shows a decrease of subsurface nitrate concentrations by about 2.5 μmol l^{-1} within 200 km from the coast in the 1/45° simulation (Fig. 8b), further supporting this interpretation. These results suggest that submesoscale frontal
15   processes amplify the mesoscale effects found in previous studies (Gruber et al., 2011; Nagai et al., 2015) namely reducing PP by enhancing the downward and offshore transport of nutrients and phytoplankton biomass. In an approach similar to ours, Gruber et al. (2011) quantified the net effect of eddy-fluxes by comparing an eddy-permitting (5 km) simulation with a "non-eddy" simulation of similar resolution but with non-linear terms in the model equations set to zero. Comparing the change in nitrate between these simulations (see Fig.3f in Gruber et al., 2011) with the change in nitrate between our 1/9° and 1/45°
20   simulations (Fig. 8b) in our study shows similarities. The patterns of decreased nitrate concentrations within ~ 200 km from the coast and increased nitrate concentrations further offshore (~ 400 - 500 km) are in good agreement (not shown). The patterns of the changes in density also match and can be explained by lateral eddy-fluxes that induce a shoreward heat transport which flattens the isopycnals (Fig. 8d, Gruber et al., 2011). **More generally, Zhong and Bracco (2013) and Zhong et al. (2017) find that submesoscale frontal processes are important for the vertical tracer transports near the surface and that**
25   **vertical dispersion of Lagrangian particles strongly increases with increasing horizontal model resolution, which is also in agreement with the results of this study (Fig. 7).** Our results further agree with the idealised model results by Lévy (2003) that submesoscale frontal processes export nutrients downward and offshore in regions with relatively high surface nutrient concentrations and can thereby reduce PP. At the same time, this enhanced downward and offshore transport would actively transport fresh organic matter into the oxycline and potentially stimulate microaerobic and anaerobic activity in the upper part
30   of the offshore OMZ (Kalvelage et al., 2013, 2015). **Subduction at fronts has previously been shown in observations to be as important for organic matter export below the photic zone as gravitational sinking (Stukel et al., 2017).**

Note that these previous studies used relatively simple biogeochemical models based on the nitrogen cycle only. Our simulations with a more complex model including the iron cycle suggest that a more complex response of the biogeochemistry to changes in the dynamics is possible. In our simulations, iron limitation occurred offshore over a larger area of the domain
35   and closer to the coast in the submesoscale-permitting simulation (not shown), suggesting that iron may be even more strongly

affected by the subduction associated with submesocale filaments and fronts than NO_3. This is in line with recent findings of Browning et al. (2018), who observed iron limitation of phytoplankton growth between 73 km - 266 km from the Peruvian coastline, in contrast with nutrient replete conditions 26 km from the coast on the shelf. The authors conclude that iron is likely an important factor driving reductions in offshore phytoplankton productivity in the PCUS. This suggests that the widespread
5   occurrence of iron limitation outside the nearshore area (~ 20 km) in our simulations is realistic.

To further investigate the processes driving the iron difference in the surface layer (Fig. 8c), we computed the iron supply from the sediments in the $1/9°$ and $1/45°$ simulations. The parameterisation of this sedimentary iron input used in PISCES only depends on water depth as an indication for how well the sediment is oxygenated. Due to slightly different topographies in the $1/9°$ and $1/45°$ grids caused by spatial smoothing, the iron supply from near-surface sediments (integrated over the upper 200 m
10   of the water column that potentially supply the upwelling) is 12.8 % higher in the $1/45°$ simulation, while the total sedimentary iron input is 22.8 % lower in the $1/45°$ simulation due to a steeper shelf break. This explains the reduced iron concentrations in the $1/45°$ simulation at 200 m - 400 m depth near the shelf (Fig. 8c), but does not affect the surface dynamics. This indicates that the strong negative surface iron anomaly does not result from differences in the sediment flux but likely from an enhanced subduction of iron-rich upwelled waters due to submesoscale dynamics.

15   The Lagrangian analysis using virtual floats allowed us to reduce the complex spatial and temporal variability of coastal upwelling and determine an average biological response to upwelling and subduction. This analysis was effective for gaining insights into physical-biogeochemical interactions from relatively short simulations. Nagai et al. (2015) conducted a virtual float experiment similar to the one in this study. They reported that 30 - 40 % of floats they released in their simulation of the Californian upwelling system were subducted below 50 m after 4 - 6 months. This compares well to our estimate, although
20   their model is only mesoscale-resolving. This could be explained by differences in the respective regions that are considered: In our study we allow for upwelling inshore of the 25 kg m^{-3} isopycnal which approximately represents the upwelling front. In contrast, Nagai et al. (2015) only released floats in a narrower region within 15 km from the coast where the probability of subduction is higher. Restricting our analysis to a smaller region on the dense side of the 25.5 kg m^{-3} isopycnal, we obtain a 5.9 % larger subducted float fraction for the $1/45°$ simulation. Other possible reasons for their relatively high subducted
25   float fraction are that eddies are generally more energetic off California compared to Peru (Capet et al., 2008a) and that they diagnose the subduction of floats over a period of 3 - 4 months compared to only 20 days in our study.

In addition to the aforementioned increase in subduction between the $1/9°$ and $1/45°$ simulations, there is also a larger number of floats upwelled in the submesoscale-permitting simulation (Table 2). This is consistent with an increase of mean upwelling velocity on the shelf between 13°S and 16°S in the $1/45°$ simulation (not shown). Moreover, our results show that
30   the enhanced upwelling and subduction in the submesoscale simulation do not cancel out but lead to substantial differences in the biogeochemical tracer fields. Using a similar approach of increasing model resolution ($1/3°$ to $1/30°$) to evaluate the impact on CO_2 air-sea fluxes in the Californian EBUS, Fiechter et al. (2014) also found an upwelling increase with increasing spatial resolution (see their Fig.7) but did not propose an explanation for this particular response. One likely explanation for this difference could be the more accurately represented steep shelf in the southern part of the domain in the $1/45°$ simulation due
35   to less topography smoothing. However, the main aim of this study is to deepen the understanding of the subduction process

occuring after the upwelling. Thus it is beyond the scope of this paper to investigate in detail the reasons for the changes in mean upwelling related to refining the coastline and increasing spatial resolution.

5   Conclusions

In this study we used an integrated approach combining high-resolution biogeochemial observations and a submesoscale-permitting model simulation to quantify subduction of upwelled nitrate off Peru. Our Lagrangian analysis of the simulations indicates that 40.6 % of the nitrate upwelled near 15°S off Peru inshore of the upwelling front is subducted again and remains unused by phytoplankton, and that 43 % of the upwelled water is subducted. **Taking model biases into account we give a best estimate for subduction of upwelled nitrate off Peru between 30.5 - 40.6 %. Comparing these results with a mesoscale simulation we find that submesoscale frontal processes increase subduction of upwelled water by 10.9 % compared to mesoscale processes, increasing the associated subduction of nitrate by 13.9 % and reducing PP by about one-third.** Average surface chlorophyll concentrations are reduced by up to $1 \, \mathrm{mg \, m^{-3}}$ and subsurface nitrate concentrations are reduced by $2.5 \, \mu \mathrm{mol \, l^{-1}}$ within $200 \, \mathrm{km}$ from the coast. These results suggest that submesoscale frontal processes amplify the mesoscale effects found in previous studies (Gruber et al., 2011; Nagai et al., 2015) by enhancing the downward and offshore transport of nutrients and fresh organic matter. In addition, surface iron concentrations were lower in the submesoscale-permitting simulation, shifting the coastal ecosystem into iron limitation and reducing PP. This effect could not be seen in previous studies that used simpler biogeochemical models. Mesoscale model studies likely underestimate the reduction of PP due to eddies and filaments.

References

Alkire, M. B., Falkner, K. K., Morison, J., Collier, R. W., Guay, C. K., Desiderio, R. A., Rigor, I. G., and McPhee, M.: Sensor-based profiles of the NO parameter in the central Arctic and southern Canada Basin: New insights regarding the cold halocline, Deep-Sea Research Part I: Oceanographic Research Papers, 57, 1432–1443, https://doi.org/10.1016/j.dsr.2010.07.011, http://dx.doi.org/10.1016/j.dsr.2010.07.011, 2010.

Arévalo-Martínez, D. L., Kock, A., Löscher, C. R., Schmitz, R. A., and Bange, H. W.: Massive nitrous oxide emissions from the tropical South Pacific Ocean, Nature Geoscience, 8, 530–533, https://doi.org/10.1038/ngeo2469, 2015.

Aumont, O., Ethé, C., Tagliabue, A., Bopp, L., and Gehlen, M.: PISCES-v2: An ocean biogeochemical model for carbon and ecosystem studies, Geoscientific Model Development, 8, 2465–2513, https://doi.org/10.5194/gmd-8-2465-2015, 2015.

Barnier, B., Siefridt, L., and Marchesiello, P.: Thermal forcing for a global ocean circulation model using a three-year climatology of ECMWF analyses, Journal of Marine Systems, 6, 363–380, https://doi.org/10.1016/0924-7963(94)00034-9, 1995.

Behrenfeld, M. J. and Falkowski, P. G.: Photosynthetic rates derived from satellite-based chlorophyll concentration, Limnology and Oceanography, 42, 1–20, 1997.

Bettencourt, J. H., Lopez, C., Hernandez-Garcia, E., Montes, I., Sudre, J., Dewitte, B., Paulmier, A., and Garçon, V.: Boundaries of the Peruvian oxygen minimum zone shaped by coherent mesoscale dynamics, Nature Geoscience, 8, 937–940, https://doi.org/10.1038/ngeo2570, 2015.

Blasco, D., Maclsaac, J. J., Packard, T. T., and Dugdale, R. C.: Relationship between nitrate reductase and nitrate uptake in phytoplankton in the Peru upwelling region,, Limnology and Oceanography, 29, 275–286, https://doi.org/10.4319/lo.1984.29.2.0275, 1984.

Brady, R. X., Lovenduski, N. S., Alexander, M. A., Jacox, M., and Gruber, N.: On the role of climate modes in modulating the air – sea CO 2 fluxes in eastern boundary upwelling systems, Biogeosciences, pp. 329–346, https://doi.org/10.5194/bg-16-329-2019, 2019.

Brink, K.: The near-surface dynamics of coastal upwelling, Progress in Oceanography, 12, 223–257, https://doi.org/10.1016/0079-6611(83)90009-5, 1983.

Browning, T. J., Rapp, I., Schlosser, C., Gledhill, M., Achterberg, E. P., Bracher, A., and Le Moigne, F. A.: Influence of Iron, Cobalt, and Vitamin B12 Supply on Phytoplankton Growth in the Tropical East Pacific During the 2015 El Niño, Geophysical Research Letters, 45, 6150–6159, https://doi.org/10.1029/2018GL077972, 2018.

Bruland, K. W., Rue, E. L., Smith, G. J., and DiTullio, G. R.: Iron, macronutrients and diatom blooms in the Peru upwelling regime: Brown and blue waters of Peru, Marine Chemistry, 93, 81–103, https://doi.org/10.1016/j.marchem.2004.06.011, 2005.

Capet, X., Colas, F., Penven, P., Marchesiello, P., and McWilliams, J. C.: Eddies in eastern-boundary subtropical upwelling systems, Ocean Modeling in an Eddying Regime, 1567, 131–147, 2008a.

Capet, X., McWilliams, J. C., Molemaker, M. J., and Shchepetkin, a. F.: Mesoscale to Submesoscale Transition in the California Current System. Part I: Flow Structure, Eddy Flux, and Observational Tests, Journal of Physical Oceanography, 38, 29–43, https://doi.org/10.1175/2007JPO3671.1, 2008b.

Capet, X. J., Marchesiello, P., and McWilliams, J. C.: Upwelling response to coastal wind profiles, Geophysical Research Letters, 31, https://doi.org/10.1029/2004GL020123, 2004.

Carr, S. D., Capet, X. J., McWilliams, J. C., Pennington, J. T., and Chavez, F. P.: The influence of diel vertical migration on zooplankton transport and recruitment in an upwelling region: Estimates from a coupled behavioral-physical model, Fisheries Oceanography, 17, 1–15, https://doi.org/10.1111/j.1365-2419.2007.00447.x, 2008.

Chaigneau, A., Dominguez, N., Vasquez, L., Flores, R., Grados, C., and Echevin, V.: Near-coastal circulation in the Northern Humboldt Current System from shipboard ADCP data, Journal of Geophysical Research, 118, 5251–5266, https://doi.org/10.1002/jgrc.20328, 2013.

Chavez, F. P., Takahashi, T., Cai, W. J., Friederich, G., Hales, B., Wanninkhof, R., and Feely, R. A.: Coastal oceans, The First State of the Carbon Cycle Report (SOCCR): The North American Carbon Budget and Implications for the Global Carbon Cycle, pp. 157–166, 2007.

5   Chavez, F. P., Bertrand, A., Guevara-Carrasco, R., Soler, P., and Csirke, J.: The northern Humboldt Current System: Brief history, present status and a view towards the future, Progress in Oceanography, 79, 95–105, https://doi.org/10.1016/j.pocean.2008.10.012, 2008.

Chelton, D. B., Deszoeke, R. A., Schlax, M. G., El Naggar, K., and Siwertz, N.: Geographical variability of the first baroclinic Rossby radius of deformation, Journal of Physical Oceanography, 28, 433–460, https://doi.org/10.1175/1520-0485(1998)028<0433:GVOTFB>2.0.CO;2, 1998.

10   Colas, F., McWilliams, J. C., Capet, X., and Kurian, J.: Heat balance and eddies in the Peru-Chile current system, Climate Dynamics, 39, 509–529, https://doi.org/10.1007/s00382-011-1170-6, 2012.

Dengler, A. T.: Relationship between physical and biological processes at an upwelling front off Peru, 15°S, Deep Sea Research Part A, Oceanographic Research Papers, 32, 1301–1315, https://doi.org/10.1016/0198-0149(85)90050-0, 1985.

Dengler, M. and Sommer, S.: Coupled benthic and pelagic oxygen, nutrient and trace metal cycling, ventilation and carbon degradation in

15   the oxygen minimum zone of the Peruvian continental margin (SFB 754): Cruise No. M 136 11.04. ? 03.05.2017 Callao (Peru) ? Callao Solute-Flux Peru, Cruise Report doi:10.3289/CR_M136, Kiel, Germany, https://doi.org/doi:10.3289/CR_M136, http://oceanrep.geomar.de/48201/, 2017.

Dugdale, R. C. and Goering, J. J.: Uptake of New and Regenerated Forms of Nitrogen in Primary Productivity, Limnology and Oceanography, 12, 196–206, https://doi.org/10.4319/lo.1967.12.2.0196, http://dx.doi.org/10.4319/lo.1967.12.2.0196, 1967.

20   Echevin, V., Aumont, O., Ledesma, J., and Flores, G.: The seasonal cycle of surface chlorophyll in the Peruvian upwelling system: A modelling study, Progress in Oceanography, 79, 167–176, https://doi.org/10.1016/j.pocean.2008.10.026, http://dx.doi.org/10.1016/j.pocean.2008.10.026, 2008.

Espinoza-Morriberon, D., Echevin, V., Colas, F., Tam, J., and Ledesma, J.: Impacts of El Niño events on the Peruvian upwelling system productivity Journal of Geophysical Research : Oceans, Journal of Geophysical Research: Oceans, https://doi.org/10.1002/2016JC012439,

25   2017.

Falkowski, P. G., Ziemann, D., Kolber, Z., and Bienfang, P. K.: Role of eddy pumping in enhancing primary production in the ocean, Nature, 352, 55–58, 1991.

Fernández, C., Farías, L., and Alcaman, M. E.: Primary production and nitrogen regeneration processes in surface waters of the Peruvian upwelling system, Progress in Oceanography, 83, 159–168, https://doi.org/10.1016/j.pocean.2009.07.010, http://dx.doi.org/10.1016/

30   j.pocean.2009.07.010, 2009.

Fiechter, J., Curchitser, E. N., Edwards, C. A., Chai, F., Goebel, N. L., and Chavez, F. P.: Air-sea CO2 fluxes in the California Current: Impacts of model resolution and coastal topography, Global Biogeochemical Cycles, 28, 371–385, https://doi.org/10.1002/2013GB004683, http://dx.doi.org/10.1002/2013GB004683, 2014.

Fonseca, T. R.: An Overview of the Poleward Undercurrent and Upwelling along the Chilean Coast, in: Poleward Flows Along Eastern Ocean

35   Boundaries, edited by Neshyba, S. J., Mooers, C. N. K., Smith, R. L., and Barber, R. T., pp. 203–228, Springer New York, New York, NY, https://doi.org/10.1007/978-1-4613-8963-7_15, https://doi.org/10.1007/978-1-4613-8963-7{_}15, 1989.

Frenger, I., Bianchi, D., Stührenberg, C., Oschlies, A., Dunne, J., Deutsch, C., Galbraith, E., and Schütte, F.: Biogeochemical Role of Subsurface Coherent Eddies in the Ocean: Tracer Cannonballs, Hypoxic Storms, and Microbial Stewpots?, Global Biogeochemical Cycles, 32, 226–249, https://doi.org/10.1002/2017GB005743, 2018.

Friederich, G. E., Ledesma, J., Ulloa, O., and Chavez, F. P.: Air-sea carbon dioxide fluxes in the coastal southeastern tropical Pacific, Progress in Oceanography, 79, 156–166, https://doi.org/10.1016/j.pocean.2008.10.001, http://dx.doi.org/10.1016/j.pocean.2008.10.001, 2008.

Grasshoff, K., Kremling, K., and Ehrhardt, M.: Methods of seawater analysis, John Wiley & Sons, 1983.

Großkopf, T., Mohr, W., Baustian, T., Schunck, H., Gill, D., Kuypers, M. M., Lavik, G., Schmitz, R. A., Wallace, D. W., and Laroche, J.: Doubling of marine dinitrogen-fixation rates based on direct measurements, Nature, 488, 361–364, https://doi.org/10.1038/nature11338, http://dx.doi.org/10.1038/nature11338, 2012.

Gruber, N.: Ocean biogeochemistry: carbon at the coastal interface, Nature, 517, 148–149, https://doi.org/10.1038/nature14082, 2015.

Gruber, N., Lachkar, Z., Frenzel, H., Marchesiello, P., Münnich, M., McWilliams, J. C., Nagai, T., and Plattner, G.-K.: Eddy-induced reduction of biological production in eastern boundary upwelling systems, Nature Geoscience, 4, 787–792, https://doi.org/10.1038/ngeo1273, http://dx.doi.org/10.1038/ngeo1273, 2011.

Gunther, E. R.: A report on oceanographical investigations in the Peru Coastal Current, Discovery Rep., 13, 107–276, http://ci.nii.ac.jp/naid/10004346955/en/, 1936.

Hauschildt, J.: Observed and modeled biogeochemistry of filaments off Peru, Master thesis, Christian-Albrechts-Universität Kiel, Kiel, Germany, https://doi.org/10.13140/RG.2.2.18259.48162, http://oceanrep.geomar.de/41369, 2017.

Hosegood, P. J., Nightingale, P., Rees, A., Widdicombe, C., Woodward, M., Clark, D., and Torres, R.: Nutrient Pumping by Submesoscale Circulations in the Mauritanian Upwelling System Nutrient Pumping by Submesoscale Circulations in the, Progress in Oceanography, https://doi.org/10.1016/j.pocean.2017.10.004, 2017.

Hutchins, D. A., Hare, C. E., Weaver, R. S., Zhang, Y., Firme, G. F., DiTullio, G. R., Alm, M. B., Riseman, S. F., Maucher, J. M., Geesey, M. E., Trick, C. G., Smith, G. J., Rue, E. L., Conn, J., and Bruland, K. W.: Phytoplankton iron limitation in the Humboldt Current and Peru Upwelling, Limnology and Oceanography, 47, 997–1011, https://doi.org/10.4319/lo.2002.47.4.0997, http://dx.doi.org/10.4319/lo.2002.47.4.0997, 2002.

Huyer, A., Knoll, M., Paluszkiewicz, T., and Smith, R. L.: The Peru Undercurrent: a study in variability, Deep Sea Research Part A. Oceanographic Research Papers, 38, S247 – S271, https://doi.org/https://doi.org/10.1016/S0198-0149(12)80012-4, http://www.sciencedirect.com/science/article/pii/S0198014912800124, 1991.

José, Y. S., Dietze, H., and Oschlies, A.: Linking diverse nutrient patterns to different water masses within anticyclonic eddies in the upwelling system off Peru, Biogeosciences Discussions, 14, 1–20, https://doi.org/10.5194/bg-2016-228, http://www.biogeosciences-discuss.net/bg-2016-228/, 2017.

Kalvelage, T., Lavik, G., Lam, P., Contreras, S., Arteaga, L., Löscher, C. R., Oschlies, A., Paulmier, A., Stramma, L., and Kuypers, M. M. M.: Nitrogen cycling driven by organic matter export in the South Pacific oxygen minimum zone, Nature Geoscience, 6, 228–234, https://doi.org/10.1038/ngeo1739, http://www.nature.com/doifinder/10.1038/ngeo1739, 2013.

Kalvelage, T., Lavik, G., Jensen, M. M., Revsbech, N. P., Löscher, C., Schunck, H., Desai, D. K., Hauss, H., Kiko, R., Holtappels, M., Laroche, J., Schmitz, R. A., Graco, M. I., and Kuypers, M. M.: Aerobic microbial respiration in oceanic oxygen minimum zones, PLoS ONE, 10, 1–17, https://doi.org/10.1371/journal.pone.0133526, http://dx.doi.org/10.1371/journal.pone.0133526, 2015.

Karstensen, J., Stramma, L., and Visbeck, M.: Oxygen minimum zones in the eastern tropical Atlantic and Pacific oceans, Progress in Oceanography, 77, 331–350, https://doi.org/10.1016/j.pocean.2007.05.009, 2008.

Köhn, E. E., Thomsen, S., Arévalo-martínez, D. L., and Kanzow, T.: Submesoscale CO 2 variability across an upwelling front off Peru, Ocean Science Discussions, pp. 1–25, 2017.

Kwiatkowski, L., Aumont, O., Bopp, L., and Ciais, P.: The Impact of Variable Phytoplankton Stoichiometry on Projections of Primary Production, Food Quality, and Carbon Uptake in the Global Ocean, Global Biogeochemical Cycles, 32, 516–528, https://doi.org/10.1002/2017GB005799, https://agupubs.onlinelibrary.wiley.com/doi/abs/10.1002/2017GB005799, 2018.

Langdon, C.: Determination of dissolved oxygen in seawater by Winkler titration using the amperometric technique, The GO-SHIP Repeat Hydrography Manual: A Collection of Expert Reports and Guidelines. Version 1, (eds Hood, E.M., C.L. Sabine, and B.M. Sloyan). 18pp.. (IOCCP Report Number 14; ICPO Publication Series Number 134), http://www.go-ship.org/HydroMan.html, 2010.

Lapeyre, G. and Klein, P.: Impact of the small-scale elongated filaments on the oceanic vertical pump, Journal of Marine Research, 64, 835–851, https://doi.org/https://doi.org/10.1357/002224006779698369, 2006.

Lathuilière, C., Echevin, V., Lévy, M., and Madec, G.: On the role of the mesoscale circulation on an idealized coastal upwelling ecosystem, Journal of Geophysical Research: Oceans, 115, 1–14, https://doi.org/10.1029/2009JC005827, 2010.

Lellouche, J. M., Greiner, E., Le Galloudec, O., Garric, G., Regnier, C., Drevillon, M., Benkiran, M., Testut, C. E., Bourdalle-Badie, R., Gasparin, F., Hernandez, O., Levier, B., Drillet, Y., Remy, E., and Le Traon, P. Y.: Recent updates to the Copernicus Marine Service global ocean monitoring and forecasting real-time 1g 12° high-resolution system, Ocean Science, 14, 1093–1126, https://doi.org/10.5194/os-14-1093-2018, 2018.

Lévy, M.: Mesoscale variability of phytoplankton and of new production: Impact of the large-scale nutrient distribution, Journal of Geophysical Research-Oceans, 108, 3358, https://doi.org/10.1029/2002JC001577, //doi.wiley.com/10.1029/2002JC001577, 2003.

Lévy, M., Ferrari, R., Franks, P. J. S., Martin, A. P., and Rivière, P.: Bringing physics to life at the submesoscale, Geophysical Research Letters, 39, 1–13, https://doi.org/10.1029/2012GL052756, 2012.

Loginova, A. N., Thomsen, S., and Engel, A.: Chromophoric and fluorescent dissolved organicmatter in and above the oxygen minimumzone off Peru, Journal of Geophysical Research: Oceans, pp. 1–18, https://doi.org/10.1002/2015JC011534.Received, 2016.

Loginova, A. N., Thomsen, S., Dengler, M., Lüdke, J., and Engel, A.: Diapycnal dissolved organic matter supply into the upper Peruvian oxycline, Biogeosciences, 16, 2033–2047, https://doi.org/10.5194/bg-16-2033-2019, 2019.

Lovecchio, E., Gruber, N., Münnich, M., and Lachkar, Z.: Mesoscale contribution to the long-range offshore transport of organic carbon from the Canary Upwelling System to the open North Atlantic, Biogeosciences, https://doi.org/10.5194/bg-14-3337-2017, 2018.

Lüdke, J., Dengler, M., Sommer, S., Clemens, D., Thomsen, S., Krahmann, G., Dale, A., Achterberg, E., and Visbeck, M.: Influence of intraseasonal eastern boundary circulation variability on hydrography and biogeochemistry off Peru, Ocean Science Discussions, 1, 1–31, https://doi.org/10.5194/os-2019-93, 2019.

Macisaac, J. J., Dugdale, R. C., Barber, R. T., and Blasco, D.: Primary production cycle in an upwelling center, Deep-Sea Research, 32, 503–529, 1985.

Mahadevan, A.: The Impact of Submesoscale Physics on Primary Productivity of Plankton, Annual review of marine science, pp. 161–184, https://doi.org/10.1146/annurev-marine-010814-015912, 2015.

Mason, E., Molemaker, J., Shchepetkin, A. F., Colas, F., McWilliams, J. C., and Sangrà, P.: Procedures for offline grid nesting in regional ocean models, Ocean Modelling, 35, 1–15, https://doi.org/10.1016/j.ocemod.2010.05.007, 2010.

McGillicuddy, D., Robinson, A., Siegel, D., Jannasch, H., Johnson, R., Dickey, T., McNeil, J., Michaels, A., and Knap, A.: Influence of mesoscale eddies on new production in the Sargasso Sea, Nature, 285, 263–266, 1998.

McWilliams, J. C.: Submesoscale currents in the ocean, Proc R. Soc. A, 472, 20160 117, http://rspa.royalsocietypublishing.org/content/472/2189/20160117, 2016.

McWilliams, J. C., Colas, F., and Molemaker, M. J.: Cold filamentary intensification and oceanic surface convergence lines, Geophysical research letters, 36, 1–5, https://doi.org/10.1029/2009GL039402, 2009.

5   McWilliams, J. C., Gula, J., Molemaker, M. J., Renault, L., and Shchepetkin, A. F.: Filament Frontogenesis by Boundary Layer Turbulence, Journal of Physical Oceanography, 45, 1988–2005, https://doi.org/10.1175/JPO-D-14-0211.1, http://journals.ametsoc.org/doi/abs/10.1175/JPO-D-14-0211.1, 2015.

Montes, I., Colas, F., Capet, X., and Schneider, W.: On the pathways of the equatorial subsurface currents in the eastern equatorial Pacific and their contributions to the Peru-Chile Undercurrent, Journal of Geophysical Research: Oceans, 115, 1–16,
10   https://doi.org/10.1029/2009JC005710, 2010.

Montes, I., Dewitte, B., Gutknecht, E., Paulmier, A., Dadou, I., Oschllies, A., and Garçon, V.: High-resolution modeling of the Eastern Tropical Pacific oxygen minimum zone: Sensitivity to the tropical oceanic circulation, Journal of Geophysical Research: Oceans, pp. 5515–5532, https://doi.org/10.1002/2014JC009858.Received, 2014.

Nagai, T., Gruber, N., Frenzel, H., Lachkar, Z., McWilliams, J. C., and Plattner, G.-K.: Dominant role of eddies and filaments in the off-
15   shore transport of carbon and nutrients in the California Current System, Journal of Geophysical Research: Oceans, pp. 5318–5341, https://doi.org/10.1002/2015JC010889.Received, 2015.

Oschlies, A.: Can eddies make ocean deserts bloom?, Global Biogeochemical Cycles, 16, 53–1–53–11, https://doi.org/10.1029/2001GB001830, http://doi.wiley.com/10.1029/2001GB001830, 2002.

Oschlies, A., Brandt, P., Stramma, L., and Schmidtko, S.: Drivers and mechanisms of ocean deoxygenation, Nature Geoscience,
20   https://doi.org/10.1038/s41561-018-0152-2, http://dx.doi.org/10.1038/s41561-018-0152-2, 2018.

Paulmier, A., Ruiz-Pino, D., Garçon, V., and Farías, L.: Maintaining of the Eastern South Pacific Oxygen Minimum Zone (OMZ) off Chile, Geophysical Research Letters, 33, 2–7, https://doi.org/10.1029/2006GL026801, 2006.

Pennington, J. T., Mahoney, K. L., Kuwahara, V. S., Kolber, D. D., Calienes, R., and Chavez, F. P.: Primary production in the eastern tropical Pacific: A review, Progress in Oceanography, 69, 285–317, https://doi.org/10.1016/j.pocean.2006.03.012, 2006.

25   Penven, P., Echevin, V., Pasapera, J., Colas, F., and Tam, J.: Average circulation, seasonal cycle, and mesoscale dynamics of the Peru Current System : A modeling approach, Journal of Geophysical Research, 110, 1–21, https://doi.org/10.1029/2005JC002945, 2005.

Penven, P., Debreu, L., Marchesiello, P., and McWilliams, J. C.: Evaluation and application of the ROMS 1-way embedding procedure to the central california upwelling system, Ocean Modelling, 12, 157–187, https://doi.org/10.1016/j.ocemod.2005.05.002, 2006.

Pietri, A., Testor, P., and Echevin, V.: Finescale Vertical Structure of the Upwelling System off Southern Peru as Observed from Glider Data,
30   Journal of Physical Oceanography, 1, 631–646, https://doi.org/10.1175/JPO-D-12-035.1, 2013.

Pietri, A., Echevin, V., Testor, P., Chaigneau, A., Mortier, L., Grados, C., and Albert, A.: Circulation of the Peru upwelling system from glider data, Journal of Geophysical Research: Oceans, 119, 2109–2120, https://doi.org/10.1002/2013JC009270.Received, 2014.

Redfield, A. C.: The influence of organisms on the composition of seawater, The sea, 2, 26–77, 1963.

Revsbech, N. P., Larsen, L. H., Gundersen, J., Dalsgaard, T., Ulloa, O., and Thamdrup, B.: Determination of ultra-low oxy-
35   gen concentrations in oxygen minimum zones by the STOX sensor, Limnology and Oceanography: Methods, 7, 371–381, https://doi.org/10.4319/lom.2009.7.371, http://doi.wiley.com/10.4319/lom.2009.7.371, 2009.

Ridgway, K. R., Dunn, J. R., and Wilkin, J. L.: Ocean interpolation by four-dimensional weighted least squares - Application to the waters around Australasia, Journal of Atmospheric and Oceanic Technology, 19, 1357–1375, https://doi.org/10.1175/1520-0426(2002)019<1357:OIBFDW>2.0.CO;2, 2002.

Rossi, V., López, C., Sudre, J., Hernández-García, E., and Garçon, V.: Comparative study of mixing and biological activity of the Benguela and Canary upwelling systems, Geophysical Research Letters, 35, 1–5, https://doi.org/10.1029/2008GL033610, 2008.

Rossi, V., López, C., Hernández-García, E., Sudre, J., Garçon, V., and Morel, Y.: Surface mixing and biological activity in the four Eastern Boundary Upwelling Systems, Nonlinear Processes in Geophysics, 16, 557–568, https://doi.org/10.5194/npg-16-557-2009, http://www.nonlin-processes-geophys.net/16/557/2009/, 2009.

Sakamoto, C. M., Johnson, K. S., and Coletti, L. J.: Improved algorithm for the computation of nitrate concentrations in seawater using an in situ ultraviolet spectrophotometer, Limnology and Oceanography-Methods, 7, 132–143, https://doi.org/10.4319/lom.2009.7.132, 2009.

Sakamoto, C. M., Johnson, K. S., Coletti, L. J., and Jannasch, H. W.: Pressure correction for the computation of nitrate concentrations in seawater using an in situ ultraviolet spectrophotometer, Limnology and Oceanography: Methods, 15, 897–902, https://doi.org/10.1002/lom3.10209, 2017.

Schmidt, M. and Eggert, A.: Oxygen cycling in the northern Benguela Upwelling System: Modelling oxygen sources and sinks, Progress in Oceanography, 149, 145–173, https://doi.org/10.1016/j.pocean.2016.09.004, http://dx.doi.org/10.1016/j.pocean.2016.09.004, 2016.

Shchepetkin, A. F. and Mcwilliams, J. C.: The regional oceanic modeling system (ROMS): a split-explicit, free-surface, topography-following-coordinate oceanic model, Ocean Modelling, 9, 347–404, https://doi.org/10.1016/j.ocemod.2004.08.002, 2005.

Shchepetkin, A. F. and McWilliams, J. C.: Computational Kernel Algorithms for Fine-Scale, Multiprocess, Longtime Oceanic Simulations, in: Handbook of Numerical Analysis: Computational Methods for the Ocean and the Atmosphere, edited by Temam, R. and Tribbia, J., vol. 14, pp. 121–183, Elsevier Science, https://doi.org/10.1016/S1570-8659(08)01202-0, http://dx.doi.org/10.1016/S1570-8659(08)01202-0, 2009.

Silva, N., Rojas, N., and Fedele, A.: Water masses in the Humboldt Current System: Properties, distribution, and the nitrate deficit as a chemical water mass tracer for Equatorial Subsurface Water off Chile, Deep-Sea Research Part II: Topical Studies in Oceanography, 56, 992–1008, https://doi.org/10.1016/j.dsr2.2008.11.001, 2009.

Smith, S. D.: Coefficients for sea surface wind stress, heat flux, and wind profiles as a function of wind speed and temperature, Journal of Geophysical Research: Oceans, 93, 15 467–15 472, 1988.

Soufflet, Y., Marchesiello, P., Lemarié, F., Jouanno, J., Capet, X., Debreu, L., and Benshila, R.: On effective resolution in ocean models, Ocean Modelling, 98, 36–50, https://doi.org/10.1016/j.ocemod.2015.12.004, 2016.

Stramma, L., Schmidtko, S., Levin, L. a., and Johnson, G. C.: Ocean oxygen minima expansions and their biological impacts, Deep-Sea Research Part I: Oceanographic Research Papers, 57, 587–595, https://doi.org/10.1016/j.dsr.2010.01.005, http://dx.doi.org/10.1016/j.dsr.2010.01.005, 2010.

Strub, P., Mesías, J., Montecino, V., Rutlant, J., and Salinas, S.: Coastal ocean circulation off western South America, 1998.

Stukel, M. R., Aluwihare, L. I., Barbeau, K. A., Chekalyuk, A. M., Goericke, R., Miller, A. J., Ohman, M. D., Ruacho, A., Song, H., Stephens, B. M., and Landry, M. R.: Mesoscale ocean fronts enhance carbon export due to gravitational sinking and subduction, Proceedings of the National Academy of Sciences, 114, 1252–1257, https://doi.org/10.1073/pnas.1609435114, http://www.pnas.org/content/114/6/1252.abstract, 2017.

Thomas, L. N., Tandon, A., and Mahadevan, A.: Submesoscale Processes and Dynamics, in: Ocean Modeling in an Eddying Regime, edited by Hecht, M. W. and Hasumi, H., pp. 17–38, American Geophysical Union, https://doi.org/10.1029/177GM04, 2008.

Thomsen, S., Kanzow, T., Colas, F., Echevin, V., Krahmann, G., and Engel, A.: Do submesoscale frontal processes ventilate the oxygen minimum zone off Peru ?, Geophysical Research Letters, pp. 8133–8142, https://doi.org/10.1002/2016GL070548.Abstract, 2016a.

Thomsen, S., Kanzow, T., Krahmann, G., Greatbatch, R. J., Dengler, M., and Lavik, G.: The formation of a subsurface anticyclonic eddy in the Peru-Chile Undercurrent and its impact on the near-coastal salinity, oxygen, and nutrient distributions, Journal of Geophysical Research: Oceans, pp. 476–501, https://doi.org/10.1002/2015JC010878.Received, 2016b.

Worley, S. J., Woodruff, S. D., Reynolds, R. W., Lubker, S. J., and Lott, N.: ICOADS release 2.1 data and products, International Journal of Climatology, 25, 823–842, https://doi.org/10.1002/joc.1166, 2005.

Wyrtki, K.: The oxygen minima in relation to ocean circulation, Deep Sea Research and Oceanographic Abstracts, 9, 11–23, https://doi.org/10.1016/0011-7471(62)90243-7, 1962.

Wyrtki, K.: The horizontal and vertical field of motion in the Peru Current, University of California Press, 1963.

Wyrtki, K.: Circulation and Water Masses in the Eastern Equatorial Pacific Ocean, Int. J. Oceanol. & Limnol. Vol, 1, 117–147, 1967.

Zhong, Y. and Bracco, A.: Submesoscale impacts on horizontal and vertical transport in the Gulf of Mexico, Journal of Geophysical Research: Oceans, 118, 5651–5668, https://doi.org/10.1002/jgrc.20402, 2013.

Zhong, Y., Bracco, A., Tian, J., Dong, J., Zhao, W., and Zhang, Z.: Observed and simulated submesoscale vertical pump of an anticyclonic eddy in the South China Sea, Scientific Reports, 7, 1–13, https://doi.org/10.1038/srep44011, 2017.

Figure S1